AIChE WILEY InterScience DISCOVER SOMETHING GREAT

Dynamic Simulation of Crystallization Processes: Adaptive Finite Element Collocation Method

Zsolt Ulbert and Béla G. Lakatos
Dept. of Process Engineering, University of Pannonia, Veszprém H 8200 Veszprém, Egyetem Str. 10, Hungary

DOI 10.1002/aic.11303
Published online October 8, 2007 in Wiley InterScience (www.interscience.wiley.com).

An adaptive orthogonal collocation on finite elements method with adaptively varied upper bound of the relevant size interval is developed for numerical solution of population balance equation of crystallizers. Nucleation producing monosized and heterosized nuclei, size-dependent crystal growth, seeding, classified product removal and fines removal with dissolution are included into the model. Adaptation of the number and length, as well as the distribution of finite elements over the variable length computational interval is carried out forming a number of adaptation rules, based on ordering the finite elements of size coordinate according to the maxima of first derivatives of the population density function. The approximation is obtained using the Lagrange interpolation polynomials. The method is used for solving the mixed set of nonlinear ordinary and partial differential equations, forming a detailed dynamical model of continuous crystallizers with product classification and/or fines removal. The program can be used efficiently for simulation of stationary and dynamic processes of crystallization systems, computing either transients or long-time oscillating steady states generated by different nonlinear phenomena, and internal and external feedbacks.
 AIChE J, 53: 3089–3107, 2007
Keywords: crystallization, population balance model, numerical solution, orthogonal collocation on finite elements, dynamic simulation

Introduction

The population balance model is an adequate mathematical description of crystallization processes. This model consists of a mixed set of ordinary and partial integrodifferential equations even in the simplest case of MSMPR (mixed suspension, mixed product removal) crystallizers, and the crucial point of using this modeling approach is the numerical solution of the population balance equation.

A number of numerical methods have been proposed for solving this equation, focusing on different modeling aspects of disperse systems, among which the weighted residual methods have received considerable attention. Subramanian and Ramkrishna,[1] considering microbial populations, were the first to use the method of weighted residuals for population balance equation, showing that the Laguerre functions were suitable trail functions on semi-infinite interval $[0, \infty)$. Singh and Ramkrishna[2] proposed problem-specific polynomials to obtain solutions to dynamic population balance problems. Lakatos et al.[3] applied the generalized Laguerre functions for simulation of batch crystallization processes, solving the population balance equation by means of orthogonal collocation, and making possible of modifying the distribution of collocation points along the size coordinate by varying the scale factor. Witkowski and Rawlings,[4] investigating identification and control issues of solution crystallizers, applied the Laguerre polynomials for computing the crystal-size distribution.

Correspondence concerning this article should be addressed to B. G. Lakatos at lakatos@fmt.uni-pannon.hu
Current address of Z. Ulbert: University of Kaposvár, Kaposvár, H. 7400 Guba Sándor Str. 40, Hungary; e-mail: ulbert@ke.hu.

Transforming the semi-infinite interval into a scaled finite one, orthogonal collocation on finite elements was applied by Gelbard and Seinfeld[5] to compute the transient processes of coagulation. Hwang and Shih[6] applied block pulse functions, while Chang and Wang[7] used the shifted Legendre functions for computing crystallization considering also the binary equal breakage. Eyre et al.[8] developed a spline-collocation method with adaptive mesh grading to compute coalescence and agglomeration processes, while Steemson and White[9] applied piecewise cubic splines for computing the steady state crystal-size distribution of continuous MSMPR crystallizers. Varga and Lakatos[10] proposed an orthogonal collocation on finite elements scheme to simulate batch grinding processes, transforming the integral with variable lower limit into definite integral with constant limits on both sides, while Canu[11] solved that problem approximating the population density function by a weighted sum of beta-distributions. Nicmanis and Hounslow[12] used finite elements of lengths generated according to geometrical progression applying Galerkin and collocation methods for computing steady states of continuous MSMPR crystallizers. Marchisio et al.[13] have showed the applicability of the quadrature method of moments, first proposed by McGraw[14] for simulating precipitation processes. A generalization and detailed investigation of the quadrature method of moments and its relationships with the method of weighted residuals have been presented recently by Grosch et al.[15] and Dorao and Jacobsen.[16] Alexopoulos et al.[17] developed an orthogonal collocation on finite elements method, and compared that with the discretization technique for solution of the dynamic population balance equation population balance equation.

The discretization techniques for numerical solution of the population balance equation have applied considerable attention also in studying crystallization systems. Hounslow et al.[18] developed a discretized version of the population balance equation involving nucleation, growth and aggregation of crystals. David et al.[19] applied the method of classes for tracking the evolution of the crystal-size distribution in batch crystallization and precipitation systems. Hill and Ng[20,21] proposed discretization procedures for solving the agglomeration and breakage equations, respectively. A combination of the Lax-Wendroff and Crank-Nicholson methods was proposed by Bennett and Rohani[22] having observed that these methods by themselves have not proved satisfactory. Kostoglou and Karabelas[23,24] carried out comparative studies of low-order methods in computing growth and breakage processes, and presented an analytical treatment of breakage-diffusion population balance.[25] Efficient improvements of discretization methods were achieved by Kumar and Ramkrishna[26,27] developing the fixed and moving pivot techniques. Ramkrishna[28] presented a review of the solution methods in the framework of a comprehensive treatment of the population balance models, and Mantzaris et al.[29,30,31] carried out a detailed study of discretization, spectral and finite element methods both in one- and multidimensional cases. The cell average technique developed by Kumar et al.[32] and extended by Kostoglou,[33] for the solution of coagulation equation has proved to be an improved successful variant of discretization methods.

The relevant interval of crystal-size distribution usually covers some orders of magnitudes, so that to produce sufficient accuracy of the numerical solution of population balance equation, a large number of finite or discretization elements are required. This number, and, consequently, the orders of the resulted systems of differential or algebraic-differential equations, can be reduced significantly by applying adaptive techniques tracking the evolution of crystal-size distribution during the course of the process. Lee et al.[34] used the method of characteristics combined with adaptive mesh generation studying seeded batch crystallization with agglomeration and breakage. The problem of handling moving sharp fronts, arising in the size distribution of crystals due to crystal growth and agglomeration processes, was addressed by Liu and Cameron[35] presenting a wavelet-based collocation method for nucleation, growth and agglomeration. The possibility of accurate front tracking was studied also by Lim et al.[36] comparing a modified method of characteristics, and a finite difference with weighted, nonoscillatory method, taking into consideration nucleation, growth, agglomeration, and breakage in batch crystallization. Mahoney and Ramkrishna[37] developed two refined Galerkin methods for efficient solution of population balance equations, with discontinuities caused by initial conditions and nucleation of crystals in precipitation.

Tracking steep moving fronts arising in crystal-size distribution provide especially important and complex modeling and computational problems when investigating dynamic phenomena in continuous crystallizers. Such oscillations are often induced by the kinetic nonlinearities and their interactions with the size distribution of crystals,[38,39,40,41,42,43,68] or due to the complex configuration of crystallizing systems involving classified product removal and/or fines destruction with the purpose of improving the quality of the crystalline product.[38,44,45] What is more, when step-like or impulse changes occur in the inputs of continuously operated crystallizers than sharp fronts or large impulses, influenced significantly by the dynamics of the crystallizer system itself, may move along the size coordinate while the real global size interval covers some orders of magnitudes. Besides, in the initial periods of startup of continuous crystallizers the relevant size interval of population density function is very small, and usually increases many orders of magnitudes during the course of the process before achieving a stationary or oscillating steady state. Therefore, when computing processes of crystallizers under such conditions, apart from tracking steep moving fronts, varying also the global size interval adaptively according to the computational requirements seems to be of great importance.

Although a lot of different aspects of dynamics of crystallizers have been considered, the problem of simulation of dynamic processes has not been addressed in its general form so far. Numerical methods for the model solution were reviewed by Rawlings et al.[46,47] showing that collocation and Galerkin's method on finite elements have proved useful tools for design and simulation of control systems of crystallizers. Kind and Nieken,[48] using a reduced model, investigated the influence of fines removal on oscillations applying the method of characteristics. Motz et al.[49] developing a detailed model of the evaporative MSMPR crystallizers, made a comparison of two methods: a finite volume scheme, and the space-time conservation element and solution element method. Puel et al.[50] applied a resolution algorithm, based on the method of classes for solving the bidimensional

population balance equation considering ideal MSMPR crystallizers. Also, the moving finite element method with time-variant adaptation[51,52] was applied by Ulbert and Lakatos[53] for solving the population balance equation under dynamic conditions. This method has proved satisfactory for that purpose, but since it was not possible to find relations between the parameters of the movement regularizing functions, and the problem to be solved, the adequate set of parameters might be obtained only by numerical experimentation. A comparison of fixed and moving grid numerical methods for dynamic evolution of the particle-size distribution was carried out by Roussos et al.[54] Wulkov et al.,[55] presented a self-adaptive solution using the Galerkin h-p method with adaptive variation of the computational size interval. A continuous evaporative MSMPR crystallizer served as a model for demonstrating the efficiency of the method in which nucleation, growth and agglomeration of crystals were included into the model. A self-adaptive finite element collocation solution was presented by Ulbert and Lakatos[56] for continuous crystallizers included into the model growth-rate dispersion, and a simple classification term. A generalized version of this solution method has proved very efficient also in studying the complex dynamic phenomena of continuous crystallizers.[57,58]

The article addresses a self-adaptive orthogonal collocation on finite elements, with adaptively varied upper bound of the relevant size interval for effective numerical solution of the population balance equation of continuous crystallizers with seeding, as well as classified product removal and fines dissolution modeled in detail as reflective recycle streams around an MSMPR crystallizer. Nucleation of monosized and heterosized nuclei and size-dependent crystal growth are included into the model. The approximation is obtained by means of the Lagrange interpolation polynomials with gradient-directed adaptation rule used in distributing the finite elements of varied number and length on the approximation interval, the global length of which is also varied adaptively depending on the predicted largest crystal size. The interior support abscissas are spaced according to the orthogonal collocation technique. The algorithm developed for solving the resulted set of algebraic-differential equations with fully adaptation is implemented in a computer program written in FORTRAN using the DAE-solver DASSL.[59]

Mathematical model

Consider a continuous isothermal crystallization system with product classification and fines removal that is represented by a network of elementary modules, treated as a combined processing system, shown in Figure 1. Let us assume that: (1) The volume of the crystal suspension in the crystallizer is constant and well mixed; (2) The crystal growth rate may be size-dependent; (3) The secondary nuclei may be monosized or heterosized, characterized by some size distribution; (4) the new monosized crystals, produced by primary and secondary nucleation formed at nominal size $L_n \cong 0$, so that we take $L_n = 0$; (5) Crystal breakage and agglomeration of crystals are negligible; (6) Product classification and fines removal are described by general selection functions $s_R(.)$ and $s_F(.)$, respectively. Then, the mathematical model of the crystallization system consists of the following equations.

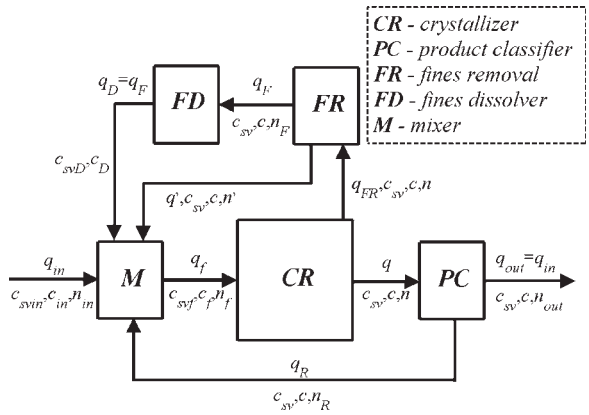

Figure 1. Crystallizer with fines removal and product classification represented as a network of elementary modules.

The variation of the population density function $n(.,.)$ is described by the population balance equation

$$\frac{\partial n(L,t)}{\partial t} + \frac{\partial [G(c,c_s,L)n(L,t)]}{\partial L} = \frac{q_{in}}{V}[n_{in}(L,t) - h(L)n(L,t)] + e_d B_d(L,c,c_s,n) \quad L \in (0,\infty), \quad t > 0 \tag{1}$$

subject to the following initial and boundary conditions

$$n(L,0) = n_0(L), \quad L \geq 0 \tag{2}$$

$$\lim_{L\to 0} G(c,c_s,L)n(L,t) = B_p(c,c_s,\varepsilon) + e_b B_b(c,c_s,\varepsilon),\ t \geq 0 \tag{3}$$

$$\lim_{L\to\infty} n(L,t) = 0, \quad t \geq 0 \tag{3b}$$

where the secondary nucleation rates B_d and B_b, selected by constraint $e_d + e_b = 1$ of binary variables e_d, $e_b \in \{0, 1\}$, are used alternatively in simulation. The primary nucleation rate B_p remains continually in simulation since it plays significant role in startup processes from clear solutions, but its influence usually is negligible in steady states.

The rates of primary and secondary nucleation B_v, $v = p,b,d$ are given by the relationships

$$B_p(c,c_s,\varepsilon) = \varepsilon k_p \exp\left(-\frac{k_e}{\ln^2\left(\frac{c}{c_s}\right)}\right) \tag{4}$$

$$B_d(L,c,c_s,n) = -S(L,c,c_s)n(L,t) + \int_L^\infty b(L,l,c)S(l,c,c_s)n(l,t)dl \tag{5}$$

and

$$B_b(c,c_s,\varepsilon) = k_b(c-c_s)^b \mu_3^j \tag{6}$$

respectively, where ε is the void fraction of the solution

$$\varepsilon(t) = 1 - k_v \int_0^\infty L^3 n(L,t)dL = 1 - k_v \mu_3(t) \tag{7}$$

and μ_3 is the third-order moment of crystal size.

The nucleation rates Eqs. 4 and 6 describe monosized nuclei, while the rate expression (Eq. 5) represents a source term of heterosized nuclei produced by contact nucleation due to collisions of crystals with different parts of crystallizer. In Eq. 5, function $S(l,c,c_s)$ provides the total number of nuclei produced by crystals of size l in unit time, and depends on the collision frequency and collision energy of crystals of different sizes, while $b(L,l)$ expresses the ratio of these nuclei falling into the size interval $(L,L+\mathrm{dL})$. Expression of such form was proposed by Ottens and de Jong[60] and Botsaris,[61] while the initial size distribution of secondary nuclei was measured by Garside et al.[62] Garside et al.[62] confirmed that collision crystallites were produced directly at sizes of up to at least 30 μm, and the number and size distribution of nuclei depended on the solution supersaturation. Similarly, heterosized nuclei were taken into consideration by Motz et al.[49] based on the model proposed by Gahn and Mersmann.[63]

The overall linear growth rate of crystals G is expressed as

$$G(c,c_s,L)=\frac{dL}{dt}=G_0(c,c_s)\phi(L)=k_g(c-c_s)^g\phi(L) \tag{8}$$

where function ϕ describes the size-dependence of the growth rate.

In Eq. 1, because of the configuration shown in Figure 1, and of the product and fines classification expressions

$$n_R(L,t)=s_R(L)n(L,t)\frac{q}{q_R} \tag{9}$$

and

$$n_F(L,t)=s_F(L)n(L,t)\frac{q_{FR}}{q_F} \tag{10}$$

the overall classification function is expressed as

$$h(L)=\left(1+\frac{q_R}{q_{in}}\right)[1-s_R(L)]+\frac{q_{FR}}{q_{in}}s_F(L) \tag{11}$$

Expression 11 is derived in Appendix 1.

The mass balance of solute, as it is also derived in Appendix 1, takes the form

$$\frac{dc}{dt}=\frac{q_{in}}{\varepsilon V}[\varepsilon_{in}c_{in}-\varepsilon_{out}c]+\rho(1-\varepsilon_F)\frac{q_F}{\varepsilon V}-\frac{1}{\varepsilon}R_c-\frac{c}{\varepsilon}\frac{d\varepsilon}{dt} \tag{12}$$

where

$$R_c=\rho G_0(c,c_s)\sigma,\quad \sigma=3k_v\int_0^\infty \phi(L)L^2n(L,t)dL. \tag{13}$$

Since the void fraction is governed by the equation

$$-\frac{d\varepsilon}{dt}=G_0(c,c_s)\sigma+\frac{1}{V}[q_{in}(\varepsilon-\varepsilon_{in})+q_R(\varepsilon-\varepsilon_R)-q_F(1-\varepsilon_F)] \tag{14}$$

combining Eqs. 12 and 14, we obtain the final form for the equation governing the concentration of solute

$$\frac{dc}{dt}=\frac{\varepsilon_{in}q_{in}}{\varepsilon V}(c_{in}-c)-\frac{1}{\varepsilon}(\rho-c)G_0(c,c_s)\sigma+\frac{q_F}{\varepsilon V}(\rho-c)(1-\varepsilon_F) \tag{15}$$

subject to the initial condition

$$c(0)=c_0. \tag{16}$$

Similarly, the mass balance equation for the solvent can be written in the form

$$\frac{dc_{sv}}{dt}=\frac{\varepsilon_{in}q_{in}}{\varepsilon V}(c_{svin}-c_{sv})+\frac{c_{sv}G_0\sigma}{\varepsilon}-\frac{c_{sv}q_F}{\varepsilon V}(1-\varepsilon_F) \tag{17}$$

subject to the initial condition

$$c_{sv}(0)=c_{sv0}. \tag{18}$$

Therefore, the state of the crystallizer at time $t\geq 0$ is given by the triple $[c(t),\ c_{sv}(t),\ n(.,t)]$, and its dynamics is described by the distributed parameter model formed by the mixed set of partial integrodifferential and ordinary differential equations (Eqs. 1, 15 and 17), subject to the initial and boundary conditions (Eqs. 2, 3, 16 and 18). The time evolution of this system occurs in the state space $\boldsymbol{R}^2\times\boldsymbol{N}$ that is the Descartes product of the vector space $\boldsymbol{R}^2$ of concentrations, and the function space $\boldsymbol{N}$ of the population density functions. Therefore, consideration of dynamic processes of the crystallizer in this product space requires a finite dimensional approximation of the population density function. In this case, we make it by developing an adaptive orthogonal collocation on finite elements method.

Scaling of the equations

A reasonable scaling is very important for the performance of numerical integration, since scaling influences the conditioning and stiffness of the resulted set of ordinary differential equations. The collocation solution of the partial differential equation, and when it is possible to derive, the moment equation model often lead to stiff systems of ordinary differential equations, so that it is reasonable to scale the model equations before the numerical solution.[40,64]

We define scale factors, together with the nucleation and growth rates, for all variables in connection with rewriting the governing equations in dimensionless form. Namely, we introduce the scaled, dimensionless variables and parameters as

$$f=s_n n,\quad f_{in}=s_n n_{in},\quad x_m=s_m\mu_m,\quad m=0,1,2,\ldots$$
$$y=s_c(c-c_s),\quad y_{in}=s_c(c_{in}-c_s),\quad y_{sv}=s_c c_{sv},$$
$$y_{svin}=s_c c_{svin},\quad \zeta_c=s_c(\rho_c-c_s),\quad \xi=s_t t,\quad \varsigma=s_L L,$$
$$\gamma=s_c c_s,\quad \overline{B}_p=B_p/B_{0,s},\quad \overline{B}_b=B_b/B_{0,s},\quad \overline{G}_0=G_0/G_{0,s}$$

by means of the scale factors s_n, s_c, s_L, s_t, $B_{0,s}$ $G_{0,s}$ and s_0, s_1, s_2 and s_3, selected appropriately for the population density function, concentrations, crystal size, time, nucleation rate, crystal growth rate and moments of crystal size, μ_0, μ_1, μ_2 and μ_3.

Choosing the scale factors

$$s_n = \frac{G_{0,s}}{B_{0,s}}, \quad s_c = \frac{1}{\max\{c_{in}\} - c_s}, \quad s_L = \frac{s_t}{G_{0,s}}, \quad s_t = \frac{1}{\bar{t}},$$
$$s_0 = 6k_v k_g^3 s_c^{-3g} s_t^{-3}, \quad s_1 = 6k_v k_g^2 s_c^{-2g} s_t^{-2},$$
$$s_2 = 3k_v k_g s_c^{-g} s_t^{-1}, \quad s_3 = k_v$$

where, $\bar{t} = V/q_{in}$ the final model takes the following dimensionless form.

Population balance equation

$$\frac{\partial f(\varsigma,\xi)}{\partial \xi} + \overline{G}_0(y)\frac{\partial[\phi(\varsigma)f(\varsigma,\xi)]}{\partial \varsigma} = f_{in}(\varsigma,\xi) - h(\varsigma)f(\varsigma,\xi)$$
$$- e_d\sigma(\varsigma,y)f(\varsigma,\xi) + e_d\int_{\varsigma}^{\infty}\beta(\varsigma,\iota,y)\sigma(\iota,y)f(\iota,\xi)d\iota, \quad \varsigma > 0, \xi > 0 \tag{19}$$

$$\lim_{\varsigma\to 0^+}\overline{G}_0\phi(\varsigma)f(\varsigma,\xi) = \overline{B}_P(y,\varepsilon) + e_b\overline{B}_b(y,\varepsilon), \quad \xi \geq 0 \tag{20}$$

$$\lim_{\varsigma\to\infty} f(\varsigma,\xi) = 0, \quad \xi \geq 0 \tag{21}$$

where

$$\sigma(\varsigma,y) = \frac{s(\varsigma,y)}{s_t}, \qquad \beta(\varsigma,\iota,y) = \frac{s_n b(\varsigma,\iota,y)}{s_L}$$

Mass balance equation for the solute

$$\frac{dy}{d\xi} = \frac{\varepsilon_{in}}{\varepsilon}(y_{in} - y) - \frac{p_1}{\varepsilon}(\zeta_c - y)y^g\int_0^{\infty}\phi(\varsigma)\varsigma^2 f(\varsigma,\xi)d\varsigma$$
$$+ \frac{p_2}{\varepsilon}\frac{q_{FR}}{q_{in}}(\zeta_c - y)\int_0^{\infty} s_F(\varsigma)\varsigma^3 f(\varsigma,\xi)d\varsigma \tag{22}$$

where the notations $p_1 = \frac{3k_v k_g}{s_t s_c^g s_n s_L^3}$ and $p_2 = \frac{k_v}{s_n s_L^4}$ were introduced.

Mass balance equation for the solvent

$$\frac{dy_{sv}}{d\xi} = \frac{\varepsilon_{in}}{\varepsilon}(y_{svin} - y_{sv}) + \frac{p_1}{\varepsilon}y_{sv}y^g\int_0^{\infty}\phi(\varsigma)\varsigma^2 f(\varsigma,\xi)d\varsigma$$
$$- \frac{p_2}{\varepsilon}\frac{q_{FR}}{q_{in}}y_{sv}\int_0^{\infty} s_F(\varsigma)\varsigma^3 f(\varsigma,\xi)d\varsigma \tag{23}$$

where

$$\varepsilon(\xi) = 1 - p_2\int_0^{\infty}\varsigma^3 f(\varsigma,\xi)d\varsigma. \tag{24}$$

Initial conditions

$$f(\varsigma,0) = f_0(\varsigma), \quad y(0) = y_0, \quad y_{sv}(0) = y_{sv0} \tag{25}$$

Kinetic equations

$$\overline{B}_p(y) = \frac{\varepsilon k_p}{B_{0,s}}\exp\left(-\frac{k_e}{\ln^2\left(\frac{y+\gamma}{\gamma}\right)}\right), \quad \overline{B}_b(y) = \frac{k_b}{s_c^b s_3^j B_{0,s}}y^b x_3^j \tag{26}$$

and

$$\overline{G}_0(y) = \frac{k_g}{s_c^g G_{0,s}}y^g \tag{27}$$

The model Eqs. 19–27 involves, as special cases, the models of

1. MSMPR (mixed suspension, mixed product removal) crystallizers with size-dependent crystal growth, and production of monosized and/or heterosized nuclei, when $q_R = 0$, $s_R(L) = 0$ and $q_{FR} = 0$,
2. MSCPR (mixed suspension, classified product removal) crystallizers when $q_{FR} = 0$.
3. MSMPR_FR (mixed suspension, mixed product removal with fines removal) crystallizers when $q_R = 0$.

Collocation equations on finite elements

In order to find a finite dimensional approximation of Eq. 19, the orthogonal collocation on finite elements method is applied as follows.

Let us assume that the maximal size of crystals, being, in principle, the upper bound of the relevant crystal-size distribution at time $\xi > 0$, is $\varsigma_{\max}(\xi)$, and let the interval $[0, \varsigma_{\max}]$ be divided into N subintervals by $N + 1$ separation nodes, shown in Figure 2, as

$$0 = \varsigma_0 < \varsigma_1 < \varsigma_2 < \ldots < \varsigma_n < \ldots < \varsigma_{N-1} < \varsigma_N = \varsigma_{\max}. \tag{28}$$

In the nth subinterval $[\varsigma_n, \varsigma_{n+1}]$, $n = 0, \ldots, N-1$, termed nth finite element, we define the local normalized size variable

$$\upsilon^n = \frac{\varsigma - \varsigma_n}{\varsigma_{n+1} - \varsigma_n}, \quad \varsigma_n \leq \varsigma \leq \varsigma_{n+1}, \quad n = 0, 1, \ldots, N-1 \tag{29}$$

and the local function $f^n(\upsilon^n, \xi)$, approximating the population density function $f(\varsigma, \xi)$ in this interval, as a linear combination of the Lagrange polynomials Λ_i^n of degree $I = 1, \ldots, I_n$

$$f^n(\upsilon^n,\xi) = \sum_{i=1}^{i=I_n} f_i^n(\xi)\Lambda_i^n(\upsilon^n), \quad n = 0, 1, \ldots, N-1 \tag{30}$$

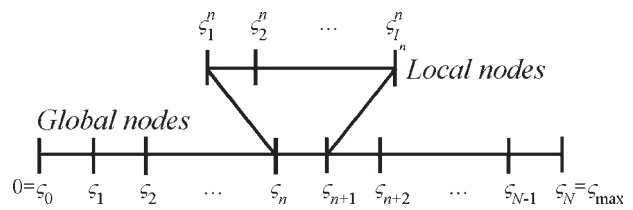

Figure 2. Finite elements on the interval [0, $\zeta\sigma_{\max}$], and the local nodes of the i^{th} element.

where

$$\Lambda_i^n(\upsilon^n)=\prod_{\substack{j=1\\ j\neq i}}^{j=I_n}\frac{\upsilon^n-\upsilon_j^n}{\upsilon_i^n-\upsilon_j^n},\quad \Lambda_i^n\left(\upsilon_j^n\right)=\delta_{i,j},$$

$$f_j^n(\xi)=f^n\left(\upsilon_j^n,\xi\right),\quad j=1,...,I_n. \quad (31)$$

and $\upsilon_j^n, j=1,\ldots,I_n$ denote the support abscissas such that if $\upsilon_1^n=0$, then $\varsigma=\varsigma_n$, and if $\upsilon_{I_n}^n=1$, then $\varsigma=\varsigma_{n+1}$, as it is shown in Figure 2.

The interior support abscissas, being also the interior collocation points of the finite elements, are chosen as the roots of the shifted Legendre polynomials of degree (I_n-2). At the internal element boundaries, the continuity of the function is imposed, at $\varsigma=0$ the boundary condition (Eq. 20) is used, while at $\varsigma=\varsigma_{\max}$ the boundary collocation is applied. As a result, the boundary value problem (Eqs. 19–21) with the first initial condition (Eq. 25) is approximated by the following system of algebraic-differential equations

$$\frac{df_j^n(\xi)}{d\xi}+\frac{\overline{G}_0(y)}{\Delta\varsigma_n}\phi\left(\frac{\upsilon_j^n\Delta\varsigma_n+\varsigma_n}{s_L}\right)\mathbf{a}_j^n\boldsymbol{f}^n(\xi)+\frac{\overline{G}_0(y)}{\Delta\varsigma_n}\frac{\partial\phi\left(\frac{\upsilon_j^n\Delta\varsigma_n+\varsigma_n}{s_L}\right)}{\partial\upsilon^n}f_j^n(\xi)$$
$$=f_{in,j}^n(\xi)-h\left(\frac{\upsilon_j^n\Delta\varsigma_n+\varsigma_n}{s_L}\right)f_j^n(\xi)-e_d\sigma\left(\upsilon_j^n\Delta\varsigma_n+\varsigma_n,y\right)f_j^n(\xi)$$
$$+e_d\left(1-\frac{\upsilon_j^n\Delta\varsigma_n+\varsigma_n}{\varsigma_{\max}}\right)\sum_{m=0}^{m=N-1}\Delta\lambda_m\sum_{i=1}^{i=I_m}\left[\sum_{k=1}^{k=K_n}w_k\chi(\upsilon_j^n\Delta\varsigma_n+\varsigma_n,$$
$$\upsilon_k^m\Delta\lambda_m+\lambda_m,y)\Lambda_i^m\left(\varsigma_{\max}-\left(1-\frac{\upsilon_j^n\Delta\varsigma_n+\varsigma_n}{\varsigma_{\max}}\right)\upsilon_k^m\right)\right]f_i^m(\xi)$$
$$n=0,1,...,N-1,\quad j=2,...,I_n \quad (32)$$

$$f_j^n(0)=f_0\left(\upsilon_j^n\Delta\varsigma_n+\varsigma_n\right),\quad n=0,1,...,N-1,\quad j=1,...,I_n \quad (33)$$

$$\overline{G}_0(y)\phi(0)f_1^0(\xi)=\overline{B}_p(y,\varepsilon)+e_b\overline{B}_b(y,\varepsilon),\quad \xi\geq 0,\quad \varsigma=\varsigma_0 \quad (34)$$

$$f_{I_n}^n(\xi)=f_1^{n+1}(\xi),\quad \xi\geq 0,\quad n=0,1,\ldots N-2 \quad (35)$$

where

$$e_d+e_b=1,\quad e_d,e_b\in\{0,1\},\quad \chi(.)=\beta(.)\sigma(.),$$
$$\Delta\varsigma_n=\varsigma_{n+1}-\varsigma_n,\quad \boldsymbol{f}^n=\left(f_1^n,f_2^n,...,f_{I_n}^n\right)^T \quad (36)$$

and the elements of vector $\boldsymbol{a}_j^n=\left(a_{j,1}^n,a_{j,2}^n,...,a_{j,I_n}^n\right)$ are

$$a_{j,i}^n=\left.\frac{d\Lambda_i^n(\upsilon^n)}{d\upsilon^n}\right|_{\upsilon_j^n}. \quad (37)$$

The scaled ordinary moments of crystal size, required in computations of mass balances of solute and solvent, are computed as

$$\mu_m(\xi)=\sum_{n=0}^{n=N-1}\left[\Delta\varsigma_n\sum_{i=1}^{i=I_n}\sum_{k=1}^{k=K_n}w_k(\upsilon_k^n\Delta\varsigma_n+\varsigma_n)^m\Lambda_i^n\left(\upsilon_k^n\right)f_i^n\right],\quad m=2,3. \quad (38)$$

The details of development of collocation Eqs. 32–38 are presented in Appendix 2.

Equations 32–36, together with the differential Eqs. 22 and 23 for mass balances of solute and solvent, form a system of algebraic-differential equations which describes the behavior of crystallization system shown in Figure 1, and can be solved by a proper integrator. However, in dynamic conditions, the particle-size distribution may exhibit sharp profiles and steep moving fronts in certain regions of the particle sizes, which often manifest as limit cycle oscillations and standing waves in steady states. Therefore, in order to minimize the number of finite elements and collocation points needed to achieve the sufficient accuracy, it is reasonable to move and place the grid points into those regions in the course of the solution where they are most efficient in approximating the exact population density function. The first step in this process is to derive appropriately the global interval of computation, and, subsequently, to distribute the finite elements along this interval adaptively.

Principles of Adaptation

Derivation of the global interval of computation

Under dynamic conditions, the maximal crystal size, i.e. the efficient support of the population density function, may change through some orders of magnitude so that the first step of the adaptation procedure is to determine the global computation interval flexibly, over which the finite elements of variable lengths are distributed. Observing the changes of the maximal crystal size in the system does this. Namely, knowing the maximal crystal size in the moment ξ we can compute its approximating value after the next time step $\Delta\xi$ as

$$\varsigma_m(\xi+\Delta\xi)\cong\varsigma_m(\xi)+\overline{G}_0(\xi)\phi[\varsigma_m(\xi)]\Delta\xi. \quad (39)$$

Then, referring to Eq. 4, we define the *Adaptation rule 1*. Let $r_1\geq 1$ be a real number, and $\varsigma_N(0)=\varsigma_{N0}$ the initial value of the upper bound of the computation interval. Then

$$\text{If } \varsigma_m(\xi+\Delta\xi)>\varsigma_N(\xi),\ \text{then } \varsigma_N(\xi+\Delta\xi)=r_1\varsigma_m(\xi+\Delta\xi),\ \text{otherwise } \varsigma_N \text{ is unchanged} \quad (40)$$

The real number r_1 is, in principle, an adjustable parameter of the adaptation. The initial value of the upper bound ς_{N0} is zero, when the crystallizer is unseeded. When, however, there is a population of seed crystals in the crystallizer at the initial moment of the process then the initial maximal size is estimated by means of Markov's inequality.

Distribution of the finite elements on the computation interval

As the upper bound of the computation interval ς_N has been fixed, the number and distribution of the finite elements along the actual computation interval are updated by examining the newly obtained population density function. The procedure developed is based on dividing the curve of the population density function into arcs of equal lengths and classification of these arc lengths with respect to the maxima of the first derivatives, as it is described by the *Adaptation rule* 2. Let *ND, NI* and $I_k>I_{NI}$, $k=1,\ldots,NI-1$, $I_{NI}=1$ be positive integer num-

bers, and $\Delta H_{\min} > 0$ be a small real number. Then the finite elements for a given ς_N is distributed according to the following steps.

Step 1. Transformation of population density function in order to equalize the range of crystal size and population density

$$\widetilde{f}(\varsigma,\xi) = \frac{f(\varsigma,\xi)\varsigma_N}{\max_{\varsigma\in[0.\varsigma_N]}\{f(\varsigma,\xi)\}} \tag{41}$$

This transformation allows standardizing the next steps of adaptation carrying out those on a square instead of rectangles having different side ratios.

Step 2. Computation of the length of the curve $H(\xi)$ of population density function by quadrature

$$H(\xi) = \int_0^{\varsigma_{\max}} \sqrt{1+\left[\frac{\partial\widetilde{f}(\varsigma,\xi)}{\partial\varsigma}\right]^2}\, d\varsigma \cong \sum_{n=0}^{n=N-1}\left[\Delta\varsigma_n k \sum_{k=1}^{k=K_n} w_j \sqrt{1+\left(\sum_{i=1}^{i=I_n}\dot{\Lambda}_i^n(\upsilon_k^n)\widetilde{f}_i^n(\xi)\right)^2}\right] \tag{42}$$

Step 3. Dividing $H(\xi)$ into *ND* arcs of equal length

$$\left\{H_j | H_j = H_k,\quad j,k = 1,...,ND,\quad H(\xi) = \bigcup_{j=1}^{ND} H_j\right\} \tag{43}$$

as it is illustrated in Figure 3a.

Dividing $H(\xi)$ into *ND* arcs of equal length and projecting the nodes separating them into the size coordinate provides by itself an efficient distribution of finite elements, distributing more finite elements at the steepest regions of the population density function. The efficiency of this method, however, can be increased by modification of these arcs according to the following steps.

Step 4. Derivation of the maximum of the first derivatives on each arc identified, and converting that into the more convenient tangent angle as a measure of steepness

$$\psi_j = arctg\left\{abs\left\{\max_{\varsigma\in H_j}\frac{\partial\widetilde{f}(\varsigma,\xi)}{\partial\varsigma}\right\}\right\},\quad j = 1,...,ND \tag{44}$$

which tangent angles vary between $0 \le \min_j\{\psi_j\} < \max_j\{\psi_j\} \le \pi/2$.

This step, i.e. introducing the tangent angle as a convenient tool of treating the problem was applied by Yu and Wang[65] for simulation of ion exchange and adsorption in fixed beds.

Step 5. Division of the interval $\min_j\{\psi_j\} < \max_j\{\psi_j\}$ into *NI* equal subintervals, as it is shown in Figure 3b

$$0 \le \min_j\{\psi_j\} = \theta_0 < \theta_1 < ... < \theta_{NI-1} < \theta_{NI} = \max_j\{\psi_j\} \le \pi/2. \tag{45}$$

and modification of the arcs obtained in *Step 3* according to the rule

$$\text{If } \psi_j \in [\theta_{k-1},\theta_k] \text{ and } \psi_l \in [\theta_{k-1},\theta_k], \text{and } H_j \text{ and } H_l \text{ are neighbours, then } H_j \text{ and } H_l \text{ are merged, } j,l = 1,...,ND \tag{46}$$

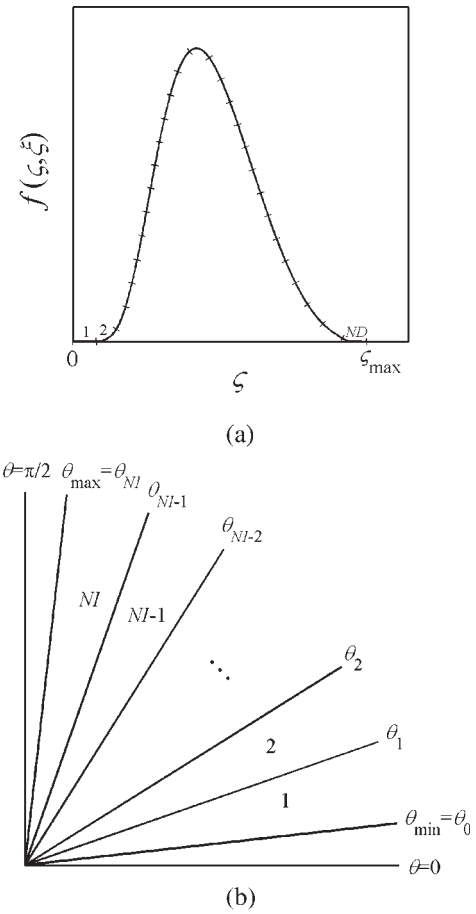

Figure 3. (a) Division of the curve of population density function into equal arc lengths, and (b) division of the interval of tangent angles.

what results in *NE* new arcs of different lengths, denoted by

$$\left\{\hat{H}_m | H(\xi) = \bigcup_{m=1}^{NE}\hat{H}_m\right\},\quad m = 1,...,NE. \tag{47}$$

In the special case of $NI = 1$ the value of *NE* equals to 1 and $\hat{H}_1 = H(\xi)$.

The results of this step is illustrated in Figure 4a and b. In these examples the value of *ND* was set to 500. The maximum of the first derivatives on each arc of transformed crystal-size distribution was determined, and the value of $\min_j\{\psi_j\} < \max_j\{\psi_j\}$ and, $j = 1,\ldots,500$, was founded as 0 and 81.63. When *NI* is selected as 2, Step 5 is resulted in four new merged arcs obtaining $NE = 4$ as it is shown in Figure 4a. In the case of $NI = 1$ all the arcs are merged as it seen in Figure 4b.

Step 6. After Step 5 we have the transformed crystal-size distribution divided into *NE* merged arcs. Each arc $\hat{H}_m, m = 1,\ldots,NE$, characterized by an interval of steepness given by Eq. 45, is divided into equal sub-arcs, by using its characteristic arc length through a minimum arc length $\Delta H_{\min}$, chosen arbitrarily, given as

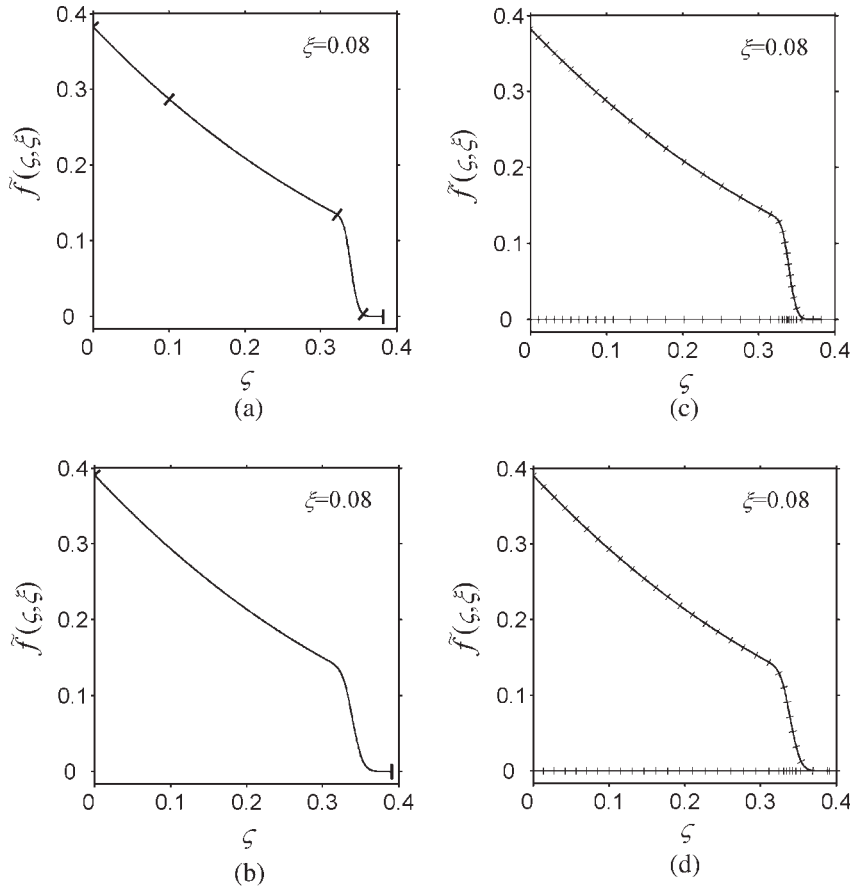

Figure 4. Procedure of division of the curve of the population density function according to the Step 5 and 6 of *Adaptation rule 2*.

$$\Delta H_k = I_k \Delta H_{\min} \tag{48}$$

and then projected the whole mesh of the curve of the population density function generated in this way into the size coordinate.

This procedure of finite element update effectively assigns the smallest elements to the regions of steepest gradients, and the largest elements to the regions of flat parts of the population density function. Here, the total number of finite elements may vary, but it seems to be reasonable to give an upper bound for their number. Giving this maximal number of elements, however, the minimal arc length $\Delta H_{\min}$ of distribution becomes also determined, fixing the number of the tangent angle intervals NI and coefficients I_k, $k = 1,\ldots,NI$. Relating to the Figure 4a and b, the final result of this procedure is illustrated in Figure 4c, when in NI is set to 2 ($\Delta H_{\min} = 0.0143$, $I_1 = 2$, $I_2 = 1$), and in Figure 4d when NI equals to 1 ($\Delta H_{\min} = 0.0194$, $I_1 = 1$).

Derivation of the moments of finite elements update

The frequency of update of the finite elements has to be large enough to follow the motion of the sharp gradients. If the update frequency is zero, then the elements will not be changed at all during the computations. When, however, this frequency is too large, then the computations require too much time. In this procedure, the moments of distributing the finite elements are determined also adaptively on the basis of the crystal growth rate. For that purpose, we introduced the following.

Adaptation rule 3. Let $r_2 \geq 1$ be a real number. Then a new distribution of the finite elements is carried out, if

1. The upper bound of the computation interval ς_N is changed, according to the *Adaptation rule 1*, or/and if
2. The computation time ξ satisfies the condition

$$\xi \geq (\xi' + \Delta\xi_a) \quad \text{where} \quad \Delta\xi_a = r_2 \min_{n=0,\ldots,N-1} \left\{ \frac{\varsigma_{n+1} - \varsigma_n}{\overline{G}_0(\xi')\phi[\varsigma_{n+1}(\xi')]} \right\} \tag{49}$$

where ξ' denotes the moment of the previous distribution of the finite elements and $\Delta\xi_a$ denotes the length of time interval to the next finite element adaptation. Here, the real number r_2 is the adjustable parameter of the rule.

Therefore, the adaptation of computations with respect to the actual properties of the population density function is based on the *Adaptation rules 1–3*. The algorithm, i.e., the sequence of steps of checking the conditions of adaptation and performing adaptation according to *Adaptation rule 2*, carried out inside of a single time step of DAE-solver is summarized in Figure 5.

The algorithm developed for solving the set of algebraic-differential Eqs. 34–36 controlled by means of *Adaptation*

Step 0. Simulation time ξ
Step 1. Computation of the next time step $\Delta\xi$
Step 2. Derivation of the maximal crystal size to refresh the computational interval
Step 4. If the condition of *Adaptation rule 1* holds then go to 8
Step 5. If the condition of *Adaptation rule 3* holds then go to 8
Step 6. Computation of the state of crystallizer at $\xi+\Delta\xi$
Step 7. $\xi:=\xi+\Delta\xi$. Go to 0
Step 8. *Adaptation rule 2*. Evaluation of the crystal size distribution and redistribution of the finite elements
Step 9. Computation of the state of crystallizer at $\xi+\Delta\xi$ using the new collocation points
Step 10. Refreshment of the condition of *Adaptation rule 3*
Step 11. $\xi:=\xi+\Delta\xi$. Go to 0

Figure 5. The algorithm of checking the conditions of adaptation and performing adaptation according to *Adaptation rule 2*, carried out inside of a single time step of DAE-solver.

rules 1–3 has been implemented in a computer program written in FORTRAN in which the DAE-solver DASSL[59] was applied. The conditions for *Adaptation rules 1–3* are checked after each integration step during the solution of Eqs. 34–36, and when a condition is satisfied the corresponding adaptation step is performed.

Implementation and simulation conditions

The kinetic expressions of crystal growth G and nucleation B_v, as well as the classification function h were included in general forms, making possible of simulation of crystallization processes under general operational conditions.

The adaptation rules involve a number of adjustableparameters: r_1, r_2, ND, NI, $\Delta H_{\min}$ and I_k, $k = 1,\ldots,NI$ by means of which the adaptation process can be designed. By means of parameters r_1 and r_2 the frequencies of the computation interval and finite element updates can be fitted to the characteristics of the problems and computational requirements. When $r_1 = 1$ and $r_2 = 1$ then the frequencies of updates are maximal so that dense elements follow the sharp gradients. At the same time, as ND or NI increases, the number of elements with different lengths also increases, so that the lengths of elements can be better adjusted for a wide range of gradients of the population density function. The division with large numbers of possible elements, however, makes the computations more complicated and time-consuming, thus, a reasonable compromise is necessary in designing the conditions of computations, providing an upper bound NS for the number of finite elements. Then, however, the parameters NS and NI determine the minimal arc length $\Delta H_{\min}$ used in the distribution. Indeed, let n_k, $k = 1,\ldots,NI$ denote the number of the primary finite elements (Eq. 43), the tangent angles of which belong to the interval $[\theta_{k-1},\theta_k]$. Obviously, $ND = \sum_{k=1}^{k=NI} n_k$. Now, the number NP_k of elements with length ΔH_k, defined by Eq. 48, is given by the following expressions

$$NP_{NI} = \left[\frac{NS}{\sum_{k=1}^{k=NI}\frac{n_k}{n_{NI}I_k}}\right] \tag{50}$$

$$NP_k = \left[\frac{n_k}{n_{NI}I_k}NP_{NI}\right], \quad k = 1,\ldots,NI-1 \tag{51}$$

where now [.] denotes the integer part of the referred quantity, and the minimal arc length is

$$\Delta H_{\min} = \frac{H}{NP_{NI}\sum_{k=1}^{k=NI}\frac{n_k}{n_{NI}}}. \tag{52}$$

The choice of the values of adaptation parameters depends on the kinetic and process parameters of crystallizers to be simulated, but the evaluation of simulation results obtained with a wide variety of process conditions has shown[57] that the tuning procedure is not too difficult. Furthermore, it has appeared that the adaptation parameters tuned to the dynamic process conditions gave large accuracy also for the approximation solutions of the stationary states compared to the analytical solutions of the population balance Eq. 19, when such solutions are known.[57]

In order to show the general capabilities of the method, however, simulation results for dynamic processes of isothermal crystallizers under comparable conditions are presented. Namely, when the size dependence of the crystal growth rate is linear, given in scaled form as

$$\phi(\varsigma) = 1 + \frac{\alpha}{s_L}\varsigma, \tag{53}$$

the fines removal is zero, i.e. $q_{FR} = 0$, and the classification function is identical with zero, i.e., $S_R(\varsigma) \equiv 0$ and $q_R = 0$, then the moment equation model of this MSMPR crystallizer becomes closed, and can be used as a system for comparing both the dynamic and stationary state solutions. When, however, the classification function of the MSCPR crystallizer is chosen as defined by Bourne and Zabelka,[66] then the stationary solution can be given in analytical form under constant concentration conditions against which the numerical solution can also be compared. This classification function, which is applied for selection function s_F also, has the following scaled form

$$s_v(\varsigma) = \frac{1 + (a/s_L^2)\varsigma^2}{1 + (b/s_L^2)\varsigma^2}, \quad a \geq 0, \quad b \geq 0, \quad v = R,F. \tag{54}$$

Since the main goal was to illustrate the capability of the method of simulating dynamic processes, the dimensionless parameters in Eqs. 19–23 were chosen in correspondence with those used by Lakatos[40] and Lakatos and Sapundzhiev,[64] studying the bifurcation and dynamic phenomena of crystallizers by means of the moment equation model. As a consequence, the nucleation rate (Eq. 4) was applied in all simulation runs presented here. The values of simulation parameters of the base case used in computations are shown in Tables 1 and 2. Therefore, in figures presenting simulation results only the actual varied parameters will be shown explicitly, since the values of the remaining parameters are taken from Tables 1 and 2.

The collocation and adaptation parameters used in the computations are shown in Table 3. Since the crystallizer was unseeded in all simulation runs, the initial values of the approximation function were given as

Table 1. Kinetic and Constitutive Parameters Used in Simulation

k_g	1.0×10^{-5} (m/h).(m^3/kg)$^{-g}$	ρ_c	1760 kg/m^3
g	1.0	k_v	0.47
k_p	8.384×10^9 no/(m^{3}h)	α	0.0
k_e	7.864×10^{-1}		

$$f_i^n(0) = 0, \quad i = 1, ..., I_n; \quad n = 0, ..., N-1 \tag{55}$$

and the computations were initiated by 50 equal finite elements given as

$$\varsigma_n = n\Delta\varsigma_0, \quad n = 0, ..., 50 \tag{56}$$

where $\Delta\varsigma_0$ denotes the initial length of the finite elements. The initial condition of the supersaturation was always $y(0) = 0.5$.

All simulation runs were carried out using a DELL personal computer developed with 1.8 GHz Intel P4 processor.

Simulation results

In the case of MSMPR crystallizers with linear size-dependent crystal growth, the accuracy of the finite element solution of dynamic processes can be checked by comparing the first four leading moments of the scaled population density function, given as

$$x_m(\xi) = \int_0^{\varsigma_{\max}} \varsigma^m f(\varsigma, \xi) d\varsigma, \quad m = 0, 1, 2, 3 \tag{57}$$

with those computed from the moment equation model having the same dimensionless para-meters, solved in each case by an ODE solver of MATLAB for stiff sets of equations. These parameter values were selected since the bifurcation analysis of the moment equation model predicted complex dynamic behavior of crystallizers in this region of system parameters, and, among those, limit cycle oscillations.[40,41]

Figures 6 and 7 show comparisons of the time variations of the moments x_3, x_4, x_5, x_6, and of the mean crystal sizes, computed from the first-order and zero-order moments as $\overline{L} = x_1 s_0 / x_0 s_1$, respectively. It is seen well that these moments computed by means of different methods have proved to be equal with great accuracy along the whole transient process, and in the steady states as well. Note that numerical solution of the population balance model predicted all lower order moments of the crystal size accurately compared with those provided by the moment equation model. The trajectories of supersaturation are shown in Figure 8 for the same parameters. Comparison of these values with those of the third-order moment presented in Figure 6, indicated that the mass balance in the numerical solution was satisfied at every moment.

Table 2. Process Parameters and Scaling Factors Used in Simulation

c_{in}	211.5 kg/m^3	$\bar{t}$	2.5 h
c_{svin}	888.5 kg/m^3	ε_{in}	1.0
c_s	130.0 kg/m^3	y_{in}	1.0
q_{in}	4 m^3/h	y_{svin}	10.9
$B_{0,s}$	1.0×10^{12} no/(m^{3}h)	$G_{0,s}$	1.0×10^{-4} (m/h) $\cdot$ (m^3/kg)$^{-g}$

Table 3. Collocation and Adaptation Parameters Used in Simulation

$I_{0,...,N-1}$	7	ND	100
r_1	1.05	NI	1
r_2	0.5	$\Delta\varsigma_0$	2.0×10^{-5}
NS	20	$K_{0,...,N-1}$	19

Three phases of development of the limit cycle oscillations of crystal-size distribution in MSMPR crystallizer are shown in Figure 9. A deep front and a large pulse of the population density function evolve in the transient states of the start-up process that are metamorphosed directly into stable steady-state oscillations representing the long-time behavior of the crystallization system. In the simulation shown in Figure 9 the processor time was equal to 623.26 s, and the finite elements were automatically redistributed by *Adaptation rules 1–3*, 1,408 times.

Two profiles of crystal-size distribution and locations of the node points during a start-up process are presented in Figure 10a and b at two moments of time, respectively, illus-

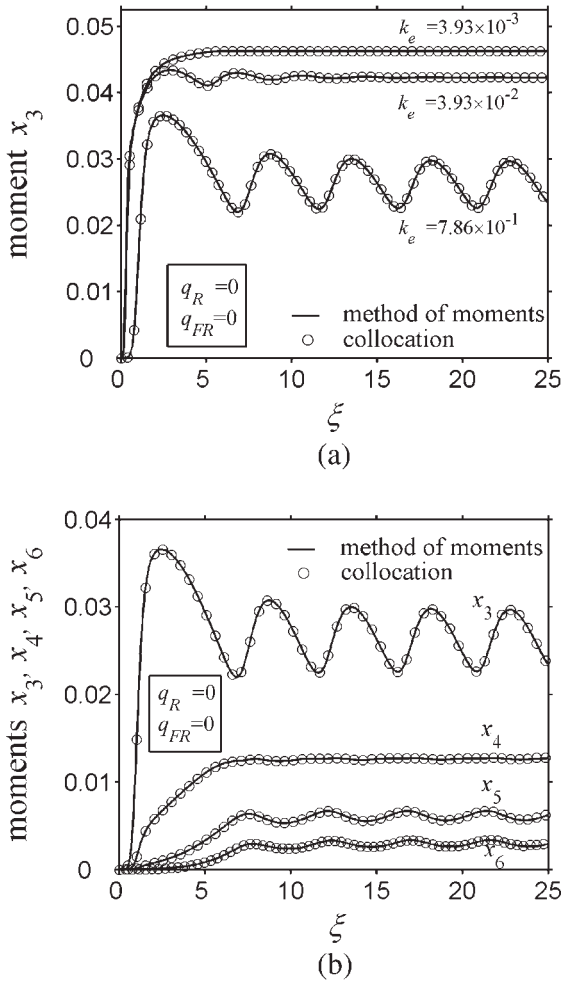

Figure 6. Comparison of the variations of the third-to sixth-order moments computed from the finite elements solution and the moment equation model.

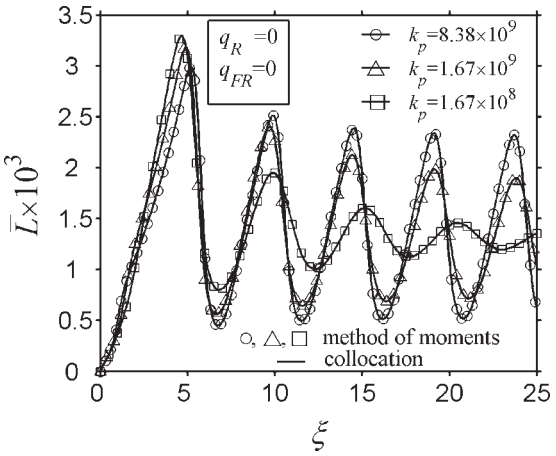

Figure 7. Comparison of variations of the mean crystal sizes computed from the finite elements solution and the moment equation model.

trating the operational efficiency of distributing the node points along the relevant size interval at different. The adaptation algorithm concentrates the finite elements and, as a consequence, the collocation points in the regions of deep gradients of the population density function of crystals. In regions where the function is flat the algorithm made use only of the maximum sized elements allowed. Evolution of the relevant computational interval and of the positions of node points as a function of time are presented in Figure 11. It is interesting to note that this figure allows following the motion of the crystal-size distribution qualitatively.

Figure 12 illustrates to some extent how the size dependence of the crystal growth, described with a monotone increasing function of size, affects the development of the crystal-size distribution. The pulse arising in the population density function becomes more flat under the influence of such size dependency.

Figure 13 presents the stabilizing effect of the size-dependent growth rate on the limit cycle oscillations as compared to those shown in Figure 9c. These simulation results confirmed

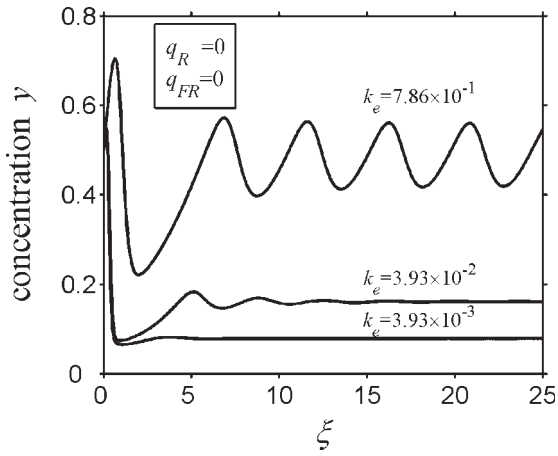

Figure 8. Variation of supersaturation as a function of time.

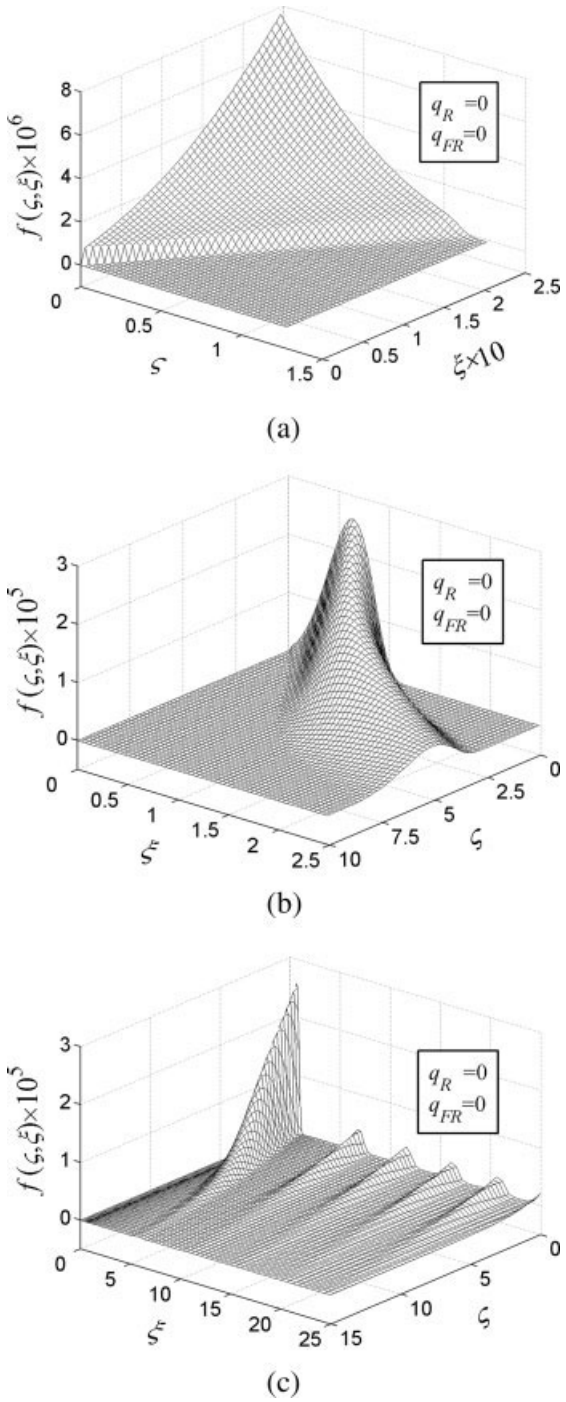

Figure 9. Development of the limit cycle oscillations of the population density function through a transient process.

the predictions obtained by means of the moment equations model regarding the influence of the size dependency of crystal growth on stability of crystallizers.[40,68]

Product classification and fines removal are important tools of improving the quality of the crystalline product, but often make the inherent inclination to instabilities of crystallizers increase. However, under certain conditions it may also

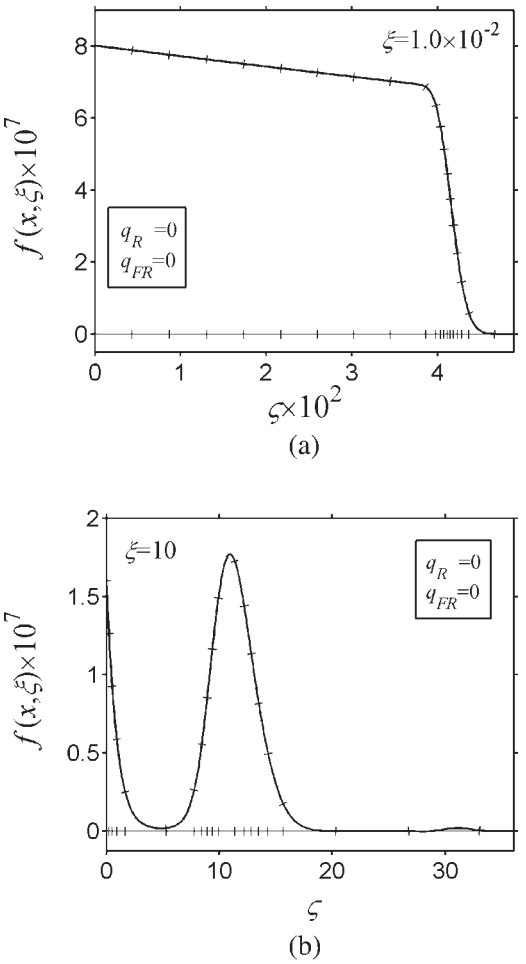

Figure 10. Profiles of the crystal-size distribution and locations of the node points during a process at two moments of time.

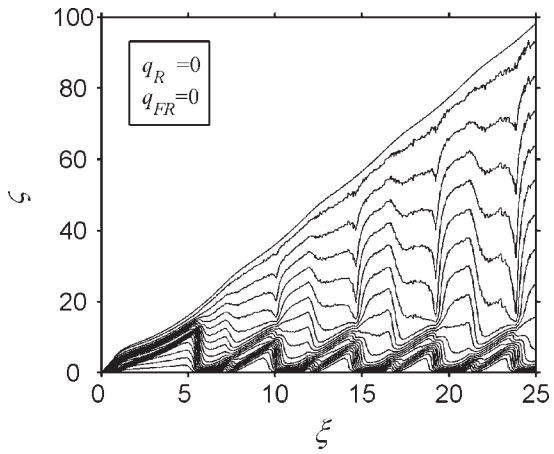

Figure 11. Positions of the computation interval and the node points as a function of time during the development of limit cycle oscillations.

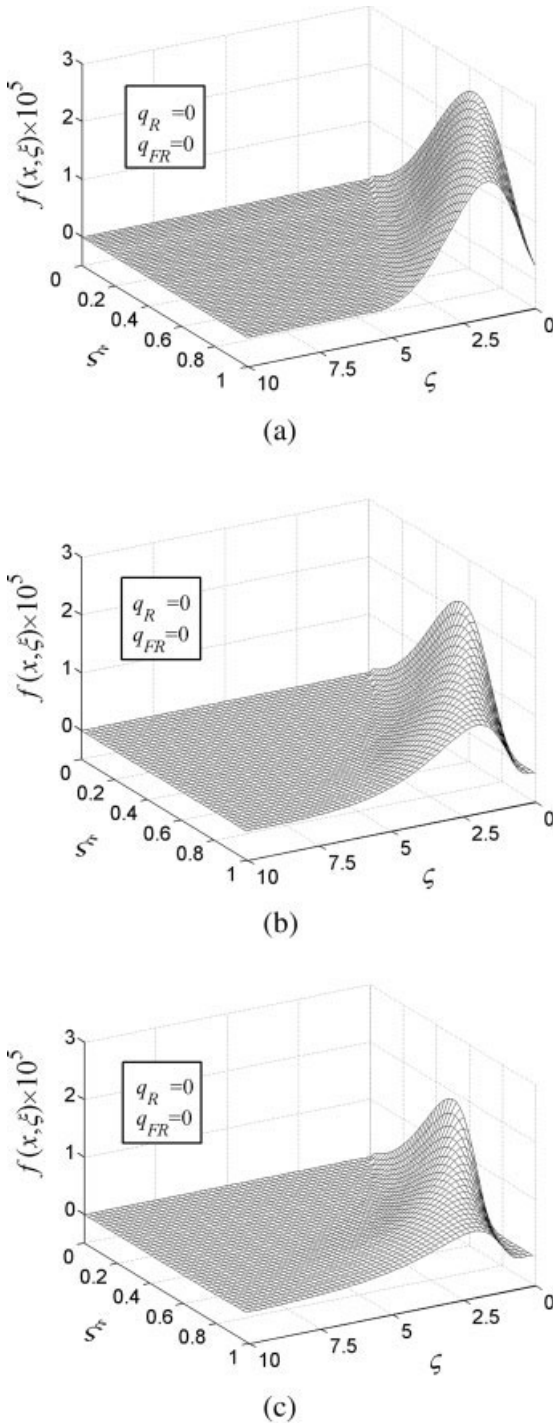

Figure 12. Effect of the size dependency of the growth rate on the development of crystal-size distribution in the interval ξ = [0, 1]: (a) α = 0; (b) α = 800; (c) α = 1,600.

damp the oscillations arising due to the nonlinearities and feedback interactions of the process.[67] Such destabilizing and stabilizing effects are presented in Figures 14–16, as compared to the limit cycle oscillations of MSMPR crystallizer shown in Figure 9c, using the nonideal classification function (Eq. 54).

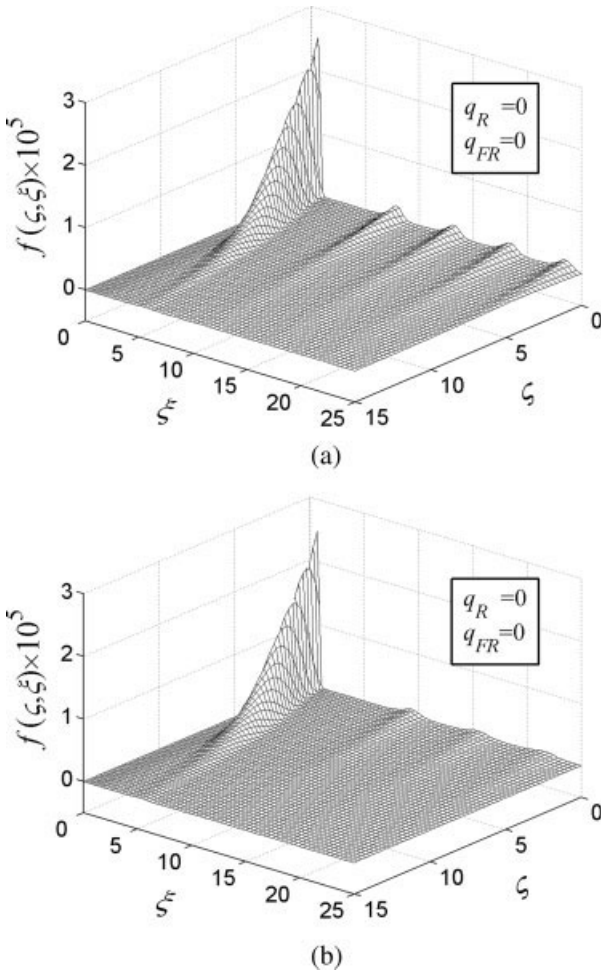

Figure 13. Stabilizing effect of the size-dependent growth rate on the limit-cycle oscillations compared to those in Figure 10c: (a) α = 100, and (b) α = 200.

Figure 14a illustrates the destabilizing effect of product classification on the long time behavior of crystallizer when $s_R(\varsigma) = \frac{1}{1+0.025\varsigma^2}$ and $q_{FR} = 0.0$. Also, the time variation of the third-order moment of crystal size is presented in Figure 14b, showing clearly that increasing the mean crystal size byproduct classification is accompanied by an increase of the amplitude and period of oscillations, and, naturally, by a decrease of the mean production rate. In this simulation run the processor time was equal to 760.53 s, and the finite elements were redistributed by *Adaptation rules 1–3*, 1,465 times.

In contrary, Figure 15 is an illustration of the stabilizing influence of the fines removal and dissolution when applying the classification function $s_F(\varsigma) = \frac{1}{1+0.025\varsigma^2}$ of the same form as before, and taking $q_R = 0.0$. The time variation of the third-order moment of crystal size is also presented in Figure 15b, showing clearly that increasing the mean crystal size byproduct classification is accompanied by increase of the amplitude and period of oscillations, and, naturally, by decrease of the mean production rate.

Finally, the resultant effects of product classification and fines destruction, applied simultaneously in the form as it was shown in Figures 14 and 15, are presented in Figure 16. Here, the fines recycled byproduct classification are removed from the crystallizer and dissolved concurrently. In this case, of the two recycle streams the destabilizing influence of product classification is the dominant effect, but decrease of the production rate expressed again as the third-order moment of crystal size is significant.

Conclusions

An adaptive orthogonal collocation on finite elements method with adaptively varying upper bound of the relevant computational size interval was developed for numerical solution of the partial integral-differential equations of population balance models of crystallizers. The mathematical model of the crystallizer system, being a mixed set of ordinary differential equations and the population balance equation, included monosized and heterosized nucleation and size-dependent growth of crystals, possible seeding, classified product removal and fines removal with dissolution of fines. Adaptation of the number and length, as well as the distribution of finite elements over the variable length computational interval was carried out forming a number of adaptation rules

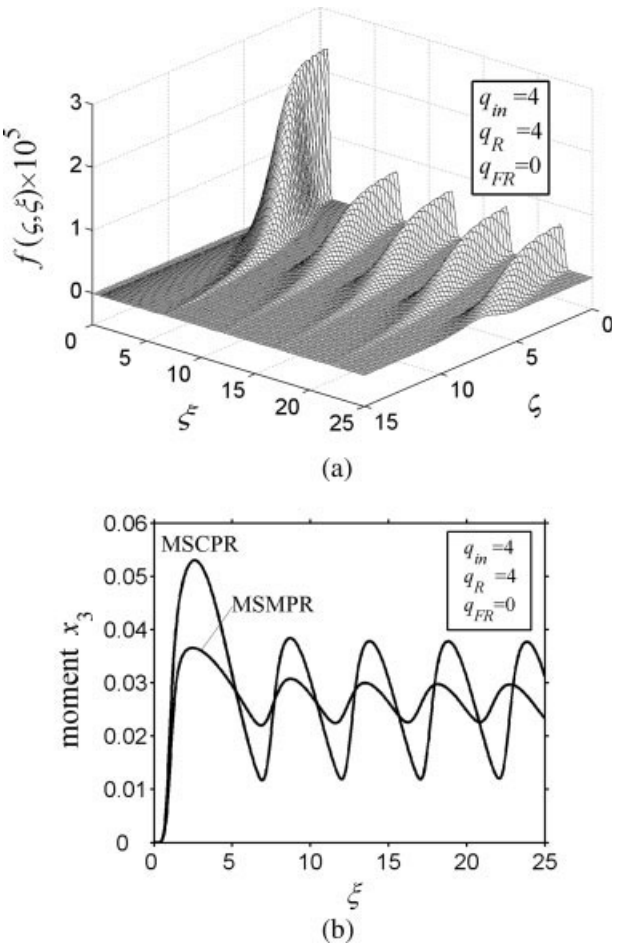

Figure 14. Destabilizing effect of the product classification in the case of classification function $S_R(\varsigma) = \frac{1}{1+0.025\varsigma^2}$.

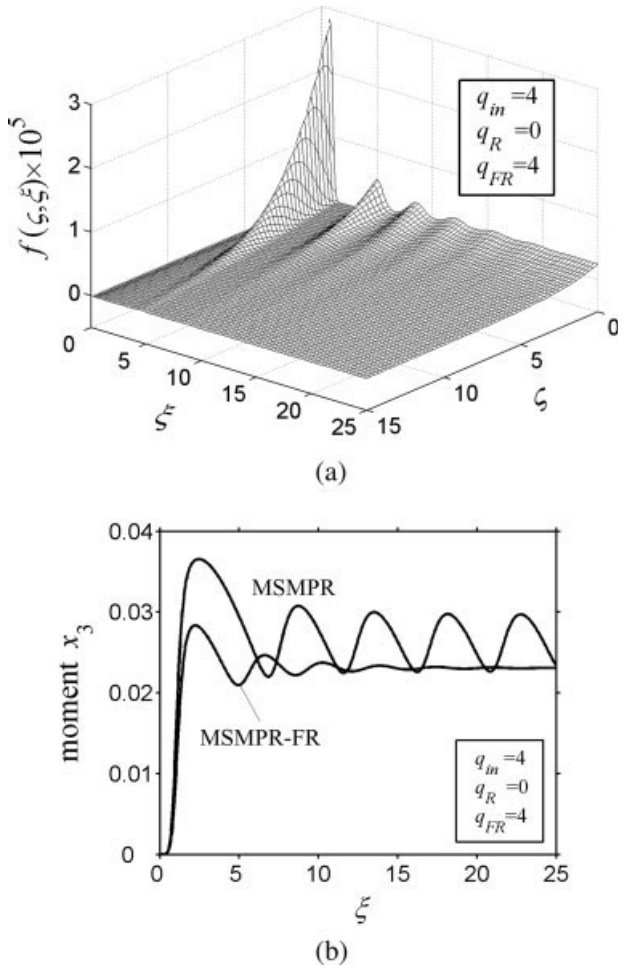

Figure 15. Stabilizing effect of fines removal and dissolution in the case of classification function $s_F(\varsigma) = \frac{1}{1+0.025\varsigma^2}$.

based on a gradient-directed method. The method is characterized with good stability and needs no additional information on the properties of crystal-size distribution.

The modeling and solution method, developed primarily with the purpose of investigating complex dynamic phenomena and processes of continuous crystallization systems, has proved an efficient tool for handling the deep gradients arising in dynamic processes of nonlinear crystallization systems even when the crystal-size distribution covers intervals differing with some orders of magnitudes. Both the start-up processes from arbitrary initial conditions, and the long-time behavior of crystallization systems, including also the steady states, are allowed tracking and computing accurately. Naturally, the model and solution method permits simulating also the dynamic processes of batch crystallizers.

The model problems applied here mostly for checking the accuracy of the method and demonstrating the capabilities of the program in simulation studies. Since analytical solutions to the population balance models of continuous crystallizers in dynamic states are not known, the corresponding moment equation models were used for comparison and checking the results. When, however, the moment equation model cannot be closed exactly then an independent check of the approximation solution was made simply by calculating the total mass of solute, which is a conserved quantity in crystallization. We note here that the rate expression of heterosized secondary nuclei is similar to that describing crystal breakage, so that this computer program can be used directly to simulate crystallization process with breakage of crystals. Since, however, crystal breakage, as well as crystal agglomeration often play significant role in crystallization and precipitation the problem of influence of breakage and agglomeration on the dynamics of crystallizers will be presented in another article.

The results of simulation runs have shown that, because of arbitrary order polynomials used on finite elements, the population density function can be interpolated accurately between the collocation points, and all important leading moments of the crystal size computed by quadrature are predicted correctly. This property makes the method capable of checking the predictions regarding the complex dynamic phenomena obtained by the moment method, as it has already been observed in the preliminary computations. Since investigation of dynamical problems of crystallizers by means of

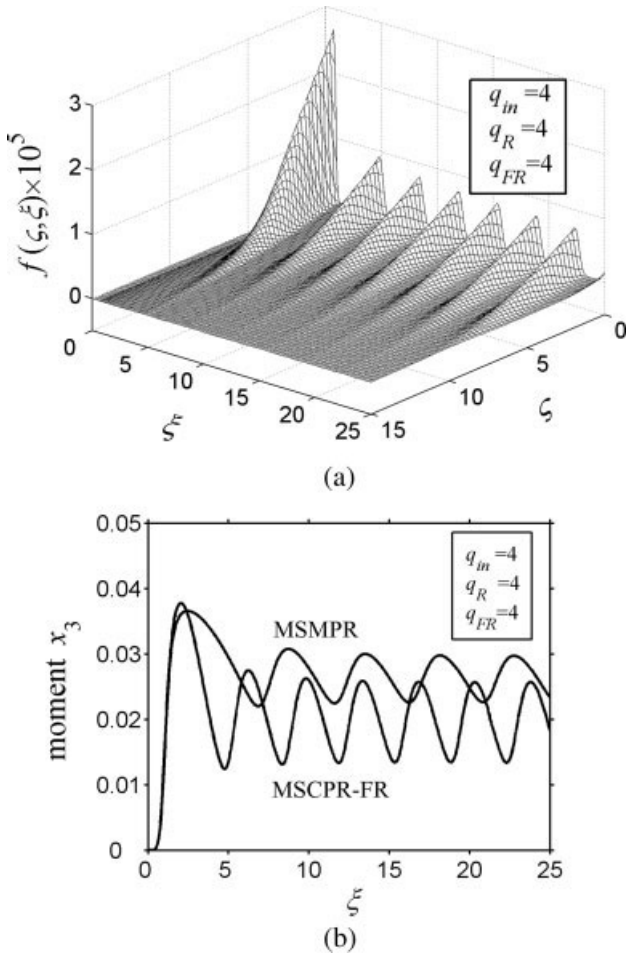

Figure 16. Resultant effect of product classification and fines removal and dissolution in the case of classification functions $s_R(\varsigma) = s_F(\varsigma) = \frac{1}{1+0.025\varsigma^2}$.

the infinite-dimensional population balance model is too complex and not constructive, and the finite-dimensional moment equation model is quite suitable for that purpose this checking capability seems to be rather useful.

In the article, focusing on presenting the principles and properties of the method, only a two-component vector, consisted of the concentration of solute and solvent under isothermal conditions, was included into the model. This part of the model of MSMPR crystallizers, however, can be extended to vectors of higher dimensions, considering the system in a more general state space $\boldsymbol{R}^k \times \boldsymbol{N}$, i.e., in the product space of $\boldsymbol{R}^k$, formed by the concentrated parameter properties of the system, and of the function space $\boldsymbol{N}$ of the population density functions. Here k is a nonnegative natural number, depending on the method of supersaturation generation. In nonisothermal cooling crystallizers with the corresponding heat balances $k = 3$, while in reaction crystallizers, where both the concentration of reactants and the volume of crystal suspension may change, the value of k may reach 6. These extensions, however, modify the total dimension of the resulted set of algebraic-ordinary differential equations only slightly compared to the dimension provided by the collocation scheme on finite element of the population balance equation.

The system configuration, consisting of an MSMPR crystallizer coupled with modeling modules of product and fines classification characterized by general classification functions is often used in technological systems as compact crystallization apparatuses that make the model and simulation program useful for analysis of operation and identification of system characteristics. Also, it has the capability of engineering design of crystallization subsystems and their control in technological systems.

Acknowledgment

The authors would like to acknowledge the support of the Hungarian Research Foundation (OTKA) under Grant T034406.

Notation

Symbols

b = exponent of nucleation rate
$\underline{B}$ = nucleation rate, no/m^{3}h
$\overline{B}$ = dimensionless nucleation rate
$B_{0,s}$ = scale factor of nucleation rate
c = concentration of solute, kg/m^3
c_s = saturation concentration of solute, kg/m^3
c_{sv} = concentration of solvent, kg/m^3
e = binary variable
f = dimensionless population density function, no/m^4
$\tilde{f}$ = transformed dimensionless population density function, no/m^4
g = exponent of crystal growth rate
G = size dependent crystal growth rate, m/h
G_0 = size independent crystal growth rate, m/h
$\overline{G}_0$ = dimensionless size independent crystal growth rate
$G_{0,s}$ = scale factor of crystal growth rate
$h(.)$ = global selection function
k_b = coefficient of the rate of nucleation, (no/m^{3}h)·(m^3/kg)$^{-b}$
k_e = parameter of primary nucleation rate
k_g = coefficient of the rate of crystal growth, (m/h)·(m^3/kg)$^{-g}$
k_p = coefficient of the rate of nucleation, (no/m^{3}h)·(m^3/kg)$^{-b}$
k_v = volumetric shape factor
L = linear crystal size, m
n = population density function of crystals, no./m^4
p_1 = parameter
p_2 = parameter
q_{FR} = volumetric rate of fines removal, m^3/h
q_{in} = volumetric rate of inlet, m^3/h
q_{out} = volumetric rate of outlet, m^3/h
q_R = volumetric rate of inlet of product classification, m^3/h
r_1, r_2 = finite element adaptation parameters
s_0 = scale factor of the 0-th moment μ_0, defined as $6k_v k_g^3 s_c^{-3g} S_t^{-3}$
s_1 = scale factor of the 1-th moment μ_1, defined as $6k_v k_g^2 s_c^{-2g} s_t^{-2}$
s_2 = scale factor of the 2-th moment μ_2, defined as $3k_v k_g s_c^{-g} s_t^{-1}$
s_3 = scale factor of the 3-th moment μ_3, defined as k_v
s_4 = scale factor of the 4-th moment μ_1, defined as $k_v k_g^{-1} s_c^g s_t/4$
s_5 = scale factor of the 5-th moment μ_2, defined as $k_v k_g^{-2} s_c^{2g} s_t^2/20$
s_6 = scale factor of the 6-th moment μ_3, defined as $k_v k_g^{-3} s_c^{3g} s_t^3/120$
s_c = scale factor of concentration, defined as $(\max\{c_{in}\} - c_s)^{-1}$
s_F = selection function of fine removal
s_L = scale factor of linear crystal size, defined as $s_t/G_{0,s}$
s_n = scale factor of population density, defined as $G_{0,s}/B_{0,s}$
s_R = selection function of product classification
s_t = scale factor of time, defined as $s_t = 1/\bar{t}$
t = time, h
$\bar{t}$ = mean residence time, h
V = volume of crystallizer, m^3
x_m = dimensionless mth order moment
y = dimensionless solute concentration
y_{sv} = dimensionless solvent concentration

Greek letters

α = parameter of the crystal growth rate, m^{-1}
η = volume fraction of solution
ϕ = function expressing the size dependency of crystal growth rate
μ_m = mth order moment of crystal size
ρ_c = crystal density, kg/m^3
γ = dimensionless saturation concentration
ς = dimensionless linear crystal size
ξ = dimensionless time
ζ_c = dimensionless crystal density

Indices

p = primary nucleation
b = secondary nucleation (boundary)
d = secondary nucleation (distributed)

Literature Cited

1. Subramanian G, Ramkrishna D. On the solution of statistical models of cell popula-tions. *Math Biosc*. 1971;10:1–23.
2. Singh PN, Ramkrishna D. Solution of population balance equations. *Comp Chem Eng*. 1977;1:23–31.
3. Lakatos B, Varga E, Halász S, Blickle T. Simulation of batch crystallizers. In: Jancic SJ, de Jong EJ. *Industrial Crystallization'84*. Amsterdam: Elsevier, 1984:185–190.
4. Witkowski WR, Rawlings, JB. Modelling and control of crystallizers. In: Proceedings of 1987 American Control Conference. Minneapolis; 1987:1–6.
5. Gelbard F, Seinfeld JW. Numerical solution of the dynamic equation for particle systems. *J Comp Physics*. 1978;28:357–375.
6. Hwang CH, Shih YP. Solution of population balance equations via block pulse func-tions. *Chem Eng J*. 1982;25:39–45.
7. Chang RY, Wang ML. Shifted Legendre function approximation of differential equations; Application to crystallization processes. *Comp Chem Eng*. 1984;8:117–125.
8. Eyre D, Wright CJ, Reuter G. Spline-collocation with adaptive mesh grading for solving the stochastic collection equation. *J Comp Physics*. 1988;78:288–304.

9. Steemson ML, White ET. Numerical modeling of steady state continuous crystallization processes using piecewise cubic spline functions. *Comp Chem Eng*. 1988;12:81–89.
10. Varga E, Lakatos B. Solution of the batch grinding equation via orthogonal colloca-tion on finite elements. *EFCE Publications Series*. 1989;74–2:563–568.
11. Canu P. Prediction of multimodal distributions in breakage processes. *Ind Eng Chem Res*. 2005;44:2649–2658
12. Nicmanis M, Hounslow MJ. Finite-element methods of steady-state population ba-lance equations. *AIChE J*. 1988;44:2258–2272.
13. Marchisio DE, Pikturna JT, Fox RO, Vigil RD, Barresi AA. Quadrature method of moments for population balance equations. *AIChE J*. 2003;49:1266–1276.
14. McGraw R. Description of aerosol dynamics by the quadrature method of moments. *Aerosol Sci Tech*. 1997;27:255–265.
15. Grosch R, Briesen H, Marquardt W, Wulkow M. Generalization and numerical investigation og QMOM. *AIChE Journal*. 2007;53:207–227.
16. Dorao CA, Jakobsen HA. The quadrature method of moments and its relationship with the method of weighted residuals. *Chem Eng Sci*. 2006;61:3327–3342.
17. Alexopoulos AH, Roussos AI, Kiparissides C. Part I: Dynamic evolution of the particle size distribution in particulate processes undergoing combined particle growth and aggregation. *Chem Eng Sci*. 2004;59:5751–5769.
18. Hounslow MJ, Ryall RL, Marshall VR. A discretized population balance for nucleation, growth and aggregation. *AIChE J*. 1988;34: 1821–1835.
19. David R, Villermaux V, Marchal P, Klein JP. Crystallization and precipitation engineering-IV. Kinetic model of adipic acid crystallization. *Chem Eng Sci*. 1991;46:1129–1136.
20. Hill PJ, Ng KM. New discretization procedure for the breakage equation. *AIChE J*. 1995;41:1204–1227.
21. Hill PJ, Ng KM. New discretization procedure for the agglomearation equation. *AIChE J*. 1996;42:727–741.
22. Bennett MK, Rohani S. Solution of population balance equations with a new combined Lax-Wendroff/Crank-Nicholson method. *Chem Eng Sci*. 2001;56:6623–6643.
23. Kostoglou M, Karabelas AJ. Evaluation of numerical methods for simulating an evolving particle size distribution in growth processes. *Chem Eng Commun*. 1995;136:177–199.
24. Kostoglou M, Karabelas AJ. An assessment of low order methods for solving the breakage equation. *Powder Technol*. 2002;127:116–127.
25. Kostoglou M, Karabelas AJ. Analytical treatment of fragmentation-diffusion population balance. *AIChE J*. 2004;50:1746–1759.
26. Kumar S, Ramkrishna D. On the solution of population balance equations by discretization—I. A fixed pivot technique. *Chem Eng Sci*. 1996;51:1311–1332.
27. Kumar S,. Ramkrishna D. On the solution of population balance equations by discretization—II. Moving pivot technique. *Chem Eng Sci*. 1996;51:1333–1342.
28. Ramkrishna D. *Population balances: Theory and applications to particulate systems in engineering*. San Diego, CA: Academic Press; 2000.
29. Mantzaris NV, Daoutidis P, Srienc F. Numerical solution of multivariable cell population balance models—I. Finite difference methods. *Comp Chem Eng*. 1995;25:1411–1440.
30. Mantzaris NV, Daoutidis P, Srienc F., Numerical solution of multivariable cell population balance models—II. Spectral methods. *Comp Chem Eng*. 1995;25:1441–1462.
31. Mantzaris NV, Daoutidis P, Srienc F. Numerical solution of multivariable cell population balance models—III. Finite element methods. *Comp Chem Eng*. 1995;25:1463–1481.
32. Kumar J, Peglow M, Warnecke G, Heinrich S, Mörl L. Improved accuracy and convergence of discretized population balance for aggregation: The cell average technique. *Chem Eng Sci*. 2006;61:3327–3342.
33. Kostoglou M. Extended cell average technique for the solution of coagulation equation. *J Colloid Interf Sci*. 2007;306:72–81.
34. Lee G, Yoon ES, Lim YI, Lann JML, Meyer XM, Joulia X. Adaptive mesh method for the simulation of crystallization processes including agglomeration and breakage: the potassium sulfite system. *Ind Eng Chem Res*. 2001;40:6228–6235.
35. Liu Y, Cameron IT. A new wavelet-based method for the solution of the population balance equation. *Chem Eng Sci*. 2001;56:5283–5294.
36. Lim YI, Lann JML, Meyer XM, Joulia X, Lee G, Yoon ES. On the solution of population balance equations with accurate front tracking methods in practical crystallization processes. *Chem Eng Sci*. 2002;57:3715–3732.
37. Mahoney AW, Ramkrishna D. Efficient solution of population balance equations with discontinuous by finite elements. *Chem Eng Sci*. 2002;57:1107–1119.
38. Randolph AD, Larson MA. *Theory of Particulate Processes*, 2nd ed. New York: Academic Press; 1988.
39. Buevich YuA, Mansurov VV, Natalukha IA. Instability and unsteady processes of the bulk continuous crystallization-I. Linear stability analysis. *Chem Eng Sci*. 1991;46:2573–2578.
40. Lakatos BG. Stability and dynamics of continuous crystallizers. *Comp Chem Eng*. 1994;18:S427–431.
41. Lakatos BG. Uniqueness and multiplicity in isothermal CMSMPR crystallizers. *AIChE Jl*. 1996;42:285–289.
42. Yin QX, Wang JK, Zhang MJ, Wang YL. Influence of nucleation mechanism on the mul-tiplicity patterns of agglomeration controlled crystallization. *Ind Eng Chem Res*. 2001;40:6221–6227.
43. Yin QX, Song YM, Wang YK. Analysis of stability and dynamic patterns of a continuous crystallizer with size-dependent crystal growth rate. *Ind Eng Chem Res*. 2003;42:630–635.
44. Eek RA, Hoogenboezem AJ, Bosgra OH. Design issues related to the control of continuous crystallizers. *Comp Chem Eng*. 1996;20:427–435.
45. Motz S, Mitrovic A, Gilles ED, Vollmer U, Raisch J. Modeling, simulation and stabilizing H_∞-control of an oscillating continuous crystallizer with fines dissolution. *Chem Eng Sci*. 2003;58:3473–3488.
46. Rawlings JB, Miller SM, Witkowski WR. Model identification and control of solution crystallization processes. *Ind Eng Chem Res*. 1993;32:1275–1296.
47. Rawlings JB, Witkowski WR, Eaton JW. Modelling and control of crystallizers. *Powder Technol*. 1992;69:3–9.
48. Kind M, Nieken U. On the dynamic simulation of mass crystallization with fines removal. *Chem Eng Proc*. 1995;34:323–328.
49. Motz S, Mitrovic A, Gilles ED. Comparison of numerical methods for the simulation of dispersed phase systems. *Chem Eng Sci*. 2002;57:4329–4344.
50. Puel F, Févotte G, Klein JP. Simulation and analysis of industrial crystallization processes through multidimensional population balance equations. *Chem Eng Sci*. 2003;58:3715–3727.
51. Miller K, Miller RN. Moving finite elements I. *SIAM J. Numer Analysis*. 1981;18:1019–1032.
52. Sereno C, Rodrigues A, Villadsen JV. The moving finite element method with polynomial approximation of any degree. *Comp Chem Eng*. 1991;15:25–33.
53. Ulbert Zs, Lakatos BG. Dynamic simulation of continuous crystallizers by moving finite elements with piecewise polynomials. In: Grievink J, van Schijdnel V. *Computer Aided Chemical Engineering-10*. Amsterdam: Elsevier; 2002a:985–990.
54. Roussos AI, Alexopoulos AH, Kiparissides C. Dynamic evolution of PSD in continuous flow processes: A comparative study of fixed and moving grid numerical techniques. *Chem Eng Sci*. 2006;61: 124–134.
55. Wulkov M, Gerstlauer A, Nieken U. Modeling and simulation of crystallization processes using Parsival. *Chem Eng Sci*. 2001;56: 2575–2588.
56. Ulbert Zs, Lakatos BG. Modelling and simulation of continuous crystallizers by adaptive finite element method. *Chem Eng Trans*. 2002b;1:1335–1340.
57. Ulbert Zs. Modelling and simulation of dynamic process of crystallizers. University of Veszprém, Veszprém, Hungary; 2003. PhD Thesis.
58. Lakatos BG. *Mathematical modeling of fluid-solids disperse systems*. Veszprém: University of Pannonia; 2005:1–180.
59. Petzold LR. A description of DASSL: a differential-algebraic system solver. In: Stepleman RS. *Scientific Computing*. Amsterdam: North Holland; 1983.
60. Ottens EPK, de Jong EJ. A model for secondary nucleation in a stirred vessel cooling crystallizer. *Kristall und Technik*. 1974;9:873–886.

61. Botsaris GD. Secondary nucleation. In: Mullin JW. *Industrial Crystallization*. New York: Plenum Press; 1976.
62. Garside J, Rusli IT, Larson MA. Origin and size distribution of secondary nuclei. *AIChE J*. 1979;25:57–65.
63. Gahn C, Mersmann A. Brittle fracture in crystallization processes. Parts A and B. *Chem Eng Sci*. 1999;54:1273–1292.
64. Lakatos BG, Sapundzhiev TsJ. Sustained oscillations in isothermal CMSMPR crystal-lizers: Effect of size-dependent crystal growth rate. *ACH—Models in Chemistry*. 1995;132:379–394.
65. Yu Q, Wang NHL. Computer simulations of the dynamics of multicomponent ion exchange and adsorption in fixed beds – gradient-directed moving finite element method. *Comp Chem Eng*. 1989;13:915–926.
66. Bourne JR. Zabelka M. The influence of gradual classification on continuous crystallization. *Chem Eng Sci*. 1980;35:533–542.
67. Lakatos BG. Nonlinear dynamics of crystallization processes. *Chem Eng Trans*. 2002;1:1149–1154.
68. Lakatos BG, Sapundzhiev TsJ, Garside J. Stability and dynamics of isothermal CMSMPR crystallizers. *Chem Eng Sci*. 2007. doi: 10.1016/j.ces.2007.04.028.

Appendix 1

Derivation of the balance equations

The continuous MSMPR crystallizer with product classification and fines removal with dissolution is treated as a combined processing system, consisted from elementary modules, as it is presented in Figure 1. This block diagram provides also a computational scheme for the system.

Let us assume that the size distribution of crystals is controlled by two classification functions: function s_R characterizing the product classification device, and function s_F describing the size distribution of the fines removed from the crystallizer during the operation. Then, the population density functions of the output, recycle and fines removal streams are given as

$$n_{out}(L,t) = [1 - s_R(L)]n(L,t)\frac{q}{q_{out}}, \quad n_R(L,t) = s_R(L)n(L,t)\frac{q}{q_R}$$

$$n_F(L,t) = s_F(L)\,n(L,t)\frac{q_{FR}}{q_F}, \;\; n'(L,t) = [1 - s_F(L)]n(L,t)\frac{q_{FR}}{q'}$$

The mass balance of solute, and the balance of volumetric rates for the block *FR* can be written as

$$\varepsilon q_{FR} c = \varepsilon_F q_F c + \varepsilon' q' c \tag{A1}$$

and

$$q_{FR} = q_F + q'. \tag{A2}$$

However, here $\varepsilon' = 0$ can be assumed, since the whole amount of the solution removed with the fines are pumped into the stream q_F. As a consequence, from Eqs. A1 and A2, we obtain

$$q_F = q_{FR}\left[1 - k_v \int_0^\infty [1 - s_F(L)]L^3 n(L,t)dL\right] \tag{A3}$$

and

$$q' = q_{FR} k_v \int_0^\infty [1 - s_F(L)]L^3 n(L,t)dL \tag{A4}$$

Since the system is assumed to be operated with constant working volume, hence, the volumetric recycle rate q_R is derived from the equalities $q = q_{out} + q_R$ and $q_{out} = q_{in}$, while the volume ratios of solution in the product and recycle streams, derived from the mass balance of crystals for the block *PC*, are given as

$$\varepsilon_{out} = 1 - k_v \int_0^\infty [1 - s_R(L)]\frac{q}{q_{in}}L^3 n(L,t)dL \tag{A5}$$

and

$$\varepsilon_R = 1 - k_v \int_0^\infty s_R(L)\frac{q}{q_R}L^3 n(L,t)dL \quad \text{and}$$

$$\varepsilon_F = 1 - k_v \int_0^\infty s_F(L)\frac{q_{FR}}{q_F}L^3 n(L,t)dL \tag{A6}$$

Now, taking into consideration that

$$q_f = q_{in} + q_R + q_F + q' \quad \text{and}$$
$$q_f n_f(L,t) = q_{in} n_{in}(L,t) + q_R n_R(L,t) + q' n'(L,t) \tag{A7}$$

as well as

$$q_f = q + q_{FR} \quad \text{and} \quad q_{FR} n(L,t) = q' n'(L,t) + q_F s_F(L) n(L,t) \tag{A8}$$

we obtain

$$\begin{aligned}\frac{\partial n(L,t)}{\partial t} + \frac{\partial [Gn(L,t)]}{\partial L} &= \frac{1}{V}[q_f n_f(L,t) - q n(L,t) - q_{FR} n(L,t)] \\ &= \frac{1}{V}[q_{in} n_{in}(L,t) + q s_R(L) n(L,t) - q n(L,t) \\ &\quad + q_{FR}(1 - s_F(L))n(L,t) - q_{FR} n(L,t)]\end{aligned} \tag{A9}$$

from which Eqs 1 and 11 follow directly. Here, $e_d = 0$ was assumed, since it has no influence on this analysis.

Similarly, because of the relations

$$\varepsilon_D q_D c_D = \varepsilon_F q_F c + \rho(1 - \varepsilon_F)q_F,$$
$$\varepsilon_D = 1, \quad c_D = \varepsilon_F c + \rho(1 - \varepsilon_F) \text{ and}$$
$$\varepsilon q c = \varepsilon_R q_R c + \varepsilon_{out} q_{out} c \tag{A10}$$

the mass balance for the solute of the crystallizer can be written as

$$\begin{aligned}V\frac{d(\varepsilon c)}{dt} &= \varepsilon_f q_f c_f - \varepsilon q c - \varepsilon q_{FR} c - V R_c \\ &= \varepsilon_{in} q_{in} c_{in} + \varepsilon_R q_R c + \varepsilon' q' c + \varepsilon_F q_F c + \rho(1 - \varepsilon_F)q_F \\ &\quad - \varepsilon_{out} q_{out} c - \varepsilon_R q_R c - \varepsilon_F q_F c - \varepsilon' q' c - V R_c \\ &= q_{in}(\varepsilon_{in} c_{in} - \varepsilon_{out} c) + \rho(1 - \varepsilon_F)q_F - V R_c\end{aligned} \tag{A11}$$

Eq. 12 can be obtained directly from A11.

Multiplying Eq. A9 by $k_v L^3$, integrating over the interval $[0,\infty)$ and rearranging, we obtain finally

$$-\frac{d\varepsilon}{dt} = 3k_v G_0(c,c_s)\int_0^\infty \phi(L)L^2 n(L,t)dL + \frac{1}{V}[q_{in}(1-\varepsilon_{in}) + q_R(1-\varepsilon_R) - q(1-\varepsilon) - q_F(1-\varepsilon_F)] \quad \text{(A12)}$$

from which Eq. 14 follows directly.

Appendix 2

Derivation of the collocation equations

Let us assume that the maximal size of crystals at time $\xi > 0$, determined by means of the Adaptation rule 1, is $\varsigma_{\max}(\xi)$. Then, assuming $\varsigma_{\max}(\xi)$ fixed, and $e_d = 1$, the population balance (Eq. 19) can be rewritten as

$$\frac{\partial f(\varsigma,\xi)}{\partial \xi} + \overline{G}_0(y)\phi(\varsigma)\frac{\partial f(\varsigma,\xi)}{\partial \varsigma} + \overline{G}_0(y)\frac{\partial \phi(\varsigma)}{\partial \varsigma}f(\varsigma,\xi) = f_{in}(\varsigma,\xi) - h(\varsigma)f(\varsigma,\xi) - \sigma(\varsigma,y)f(\varsigma,\xi) + \int_\varsigma^{\varsigma_{\max}} \beta(\varsigma,\imath,y)\sigma(\imath,y)f(\imath,\xi)d\imath \quad \text{(A13)}$$

In Eq. A13, we have a definite integral with variable lower limit. As the first step of the solution, by means of transformation

$$\lambda = \varsigma_{\max}\frac{\varsigma_{\max}-\imath}{\varsigma_{\max}-\varsigma}, \quad \imath = \varsigma_{\max} - (\varsigma_{\max}-\varsigma)\frac{\lambda}{\varsigma_{\max}}, \quad d\imath = -\left(1-\frac{\varsigma}{\varsigma_{\max}}\right)d\lambda \quad \text{(A14)}$$

this integral with variable lower limit is transformed into a definite integral with constant limits

$$\left(1-\frac{\varsigma}{\varsigma_{\max}}\right)\int_0^{\varsigma_{\max}} \beta\left(\varsigma,\varsigma_{\max}-(\varsigma_{\max}-\varsigma)\frac{\lambda}{\varsigma_{\max}},y\right) \times \sigma\left(\varsigma_{\max}-(\varsigma_{\max}-\varsigma)\frac{\lambda}{\varsigma_{\max}},y\right) \times f\left(\left(\varsigma_{\max}-(\varsigma_{\max}-\varsigma)\frac{\lambda}{\varsigma_{\max}}\right),\xi\right)d\lambda \quad \text{(A15)}$$

Introduction to the notation

$$\beta\left(\varsigma,\varsigma_{\max}-(\varsigma_{\max}-\varsigma)\frac{\lambda}{\varsigma_{\max}},y\right)\sigma\left(\varsigma_{\max}-(\varsigma_{\max}-\varsigma)\frac{\lambda}{\varsigma_{\max}},y\right) = \chi(\varsigma,\lambda,y) \quad \text{(A16)}$$

Eq. A13 can be written in the form

$$\frac{\partial f(\varsigma,\xi)}{\partial f(\xi)} + \overline{G}_0(y)\phi(\varsigma)\frac{\partial f(\varsigma,\xi)}{\partial \varsigma} + \overline{G}_0(y)\frac{\partial \phi(\varsigma)}{\partial \varsigma}f(\varsigma,\xi) = f_{in}(\varsigma,\xi) - h(\varsigma)f(\varsigma)f(\varsigma,\xi) - \sigma(\varsigma,y)f(\varsigma,\xi) + \left(1-\frac{\varsigma}{\varsigma_{\max}}\right)\int_\varsigma^{\varsigma_{\max}} \chi(\varsigma,\lambda,y)f\left(\left(\varsigma_{\max}-(\varsigma_{\max}-\varsigma)\frac{\lambda}{\varsigma_{\max}}\right),\xi\right)d\lambda \quad \text{(A17)}$$

Assuming that partition (Eq. 28), determined by means of *Adaptation rule 2*, is fixed, the continuous population density function, according to the orthogonal collocation on finite elements is approximated by the polynomial expressions as in Eq.

$$f^n(\upsilon^n,\xi) = \sum_{i=1}^{i=I_n} f_i^n(\xi)\Lambda_i^n(\upsilon^n), \quad n = 0,1,...,N-1 \quad \text{(30)}$$

over the elements (Eq. 28) as a trial function, where $f_i^n(\xi)$ denotes the value of the population density function at time ξ at the ith support abscissa of nth element, and Λ_i^n is the Lagrange polynomial of degree $I = 1,\ldots,I_n$. Since these abscissas are to be selected also as the interior collocation points in finite elements, they are chosen as the roots of the shifted Legendre polynomials of degree (I_n-2). As a consequence, such selection of collocation points allows computing the integrals by quadratures accurately.

The first derivates of the trial functions with respect to time and local coordinates (Eq. 29), considering the property (Eq. 31), are expressed as

$$\frac{\partial f^n(\upsilon^n,\xi)}{\partial \xi} = \sum_{i=1}^{i=I_n}\frac{\partial f_i^n(\xi)}{\partial \xi}\Lambda_i^n(\upsilon^n), \quad n = 0,1,...,N-1 \quad \text{(A18)}$$

and

$$\left.\frac{\partial f^n(\upsilon^n,\xi)}{\partial \upsilon^n}\right|_{\upsilon_j^n} = \sum_{i=1}^{i=I_n} a_{j,i}^n f_i^n(\xi) \quad j = 1,...,I_n, \quad n = 0,...,N-1 \quad \text{(A19)}$$

where

$$a_{j,i}^n = \left.\frac{d\Lambda_i^n(\upsilon^n)}{d\upsilon^n}\right|_{\upsilon_j^n} \quad \text{(A20)}$$

The ordinary moments in Eqs. 22 and 23 are given as special cases of moments of the scaled crystal size to some general function $g(.)$ computed as

$$\mu[g,\xi] = \int_0^{\varsigma_{\max}} g(\varsigma)f(\varsigma,\xi)d\varsigma \cong \sum_{n=0}^{n=N-1}\int_{\varsigma_n}^{\varsigma_{n+1}} g(\varsigma)f(\varsigma,\xi)d\varsigma = \sum_{n=0}^{n=N-1}\Delta\varsigma_n\int_0^1 g(\upsilon^n\Delta\varsigma_n+\varsigma_n)f(\upsilon^n\Delta\varsigma_n+\varsigma_n,\xi)d\upsilon^n \quad \text{(A21)}$$

where $\Delta\varsigma_n = \varsigma_{n+1} - \varsigma_n$.

Substituting the trial functions $f^n(\upsilon^n,\xi), n = 0,1,\ldots,N-1$, $n = 0,1,\ldots,N-1$, into Eq. A21, and applying the Lobatto quadrature with K_n quadrature points, and w_k, $k = 1,2,\ldots,K_n$ weights, we obtain

$$\mu[g,\xi] \cong \sum_{n=0}^{n=N-1}\left[\Delta\varsigma_n\sum_{k=1}^{k=K_n} w_k g(\upsilon_k^n\Delta\varsigma_n+\varsigma_n)f^n(\upsilon_k^n,\xi)\right] = \sum_{n=0}^{n=N-1}\left[\Delta\varsigma_n\sum_{i=1}^{i=I_n}\sum_{k=1}^{k=K_n} w_k g(\upsilon_k^n\Delta\varsigma_n+\varsigma_n)\Lambda_i^n(\upsilon_k^n)f_i^n\right] \quad \text{(A22)}$$

from which the approximated value of the zero-order moment is given as. $\mu_0(\xi) = \mu[1, \xi]$. In general, any ordinary moment μ_m, $m = 0, 1, 2 \ldots$ of the crystal size is computed as

$$\mu_m(\xi) = \mu[\varsigma^m, \xi], \quad m = 0, 1, 2 \ldots \tag{A23}$$

The second integral in last term on the righthand side of Eq. A13 is computed also by

$$\begin{aligned}\sum_{m=0}^{m=N-1} \Delta\lambda_m \int_0^1 \chi(\varsigma, \lambda_m + \Delta\lambda_m \upsilon^m, y) f\left(\left(\varsigma_{\max} - (\varsigma_{\max} - \varsigma)\frac{(\lambda_m + \Delta\lambda_m \upsilon^m)}{\varsigma_{\max}}\right), \xi\right) d\upsilon^m \\ = \sum_{m=0}^{m=N-1} \Delta\lambda_m \sum_{k=1}^{k=K_m} w_k \chi(\varsigma, \lambda_m + \Delta\lambda_m \upsilon_k^m, y) f^m\left(\left(\varsigma_{\max} - (\varsigma_{\max} - \varsigma)\frac{\upsilon_k^m}{\varsigma_{\max}}\right), \xi\right) \\ = \sum_{m=0}^{m=N-1} \Delta\lambda_m \sum_{k=1}^{k=K_m} w_k \chi(\varsigma, \lambda_m + \Delta\lambda_m \upsilon_k^m, y) \sum_{i=1}^{i=I_m} f_i^m(\xi) \Lambda_i^m\left(\varsigma_{\max} - (\varsigma_{\max} - \varsigma)\frac{\upsilon_k^m}{\varsigma_{\max}}\right)\end{aligned} \tag{A24}$$

Finally, substituting the trial function (Eq. 30) into Eq. A18, taking the values of trial functions at the collocation points $\upsilon_j^n, j = 1, \ldots, I_n,\ n = 0, 1, \ldots, N-1$, and taking into consideration the property (Eq. 31), and expressions (Eqs. A18– A24, the collocation equations approximating Eq. A13 becomes

$$\begin{aligned}\frac{\partial f_j^n(\xi)}{d\xi} + \frac{\overline{G}_0}{\Delta\varsigma_n}\phi\left(\frac{\upsilon_j^n \Delta\varsigma_n + \varsigma_n}{s_L}\right)\mathbf{a}_j^n \boldsymbol{f}^n(\xi) + \frac{\overline{G}_0}{\Delta\varsigma_n}\frac{\partial\phi\left(\frac{\upsilon_j^n\Delta\varsigma_n + \varsigma_n}{s_L}\right)}{\partial\upsilon^n} f_j^n(\xi) \\ = f_{in,j}^n(\xi) - h\left(\frac{\upsilon_j^n \Delta\varsigma_n + \varsigma_n}{s_L}\right) f_j^n(\xi) - \sigma\left(\varsigma_n + \Delta\varsigma_n \upsilon_j^n, y\right) f_j^n(\xi) + \left(1 - \frac{\upsilon_j^n \Delta\varsigma_n + \varsigma_n}{\varsigma_{\max}}\right) \\ \times \sum_{m=0}^{m=N-1} \Delta\lambda_m \sum_{i=1}^{i=I_m}\left[\sum_{k=1}^{k=K_n} w_k \chi(\upsilon_j^n \Delta\varsigma_n + \varsigma_n, \lambda_m + \Delta\lambda_m \upsilon_k^m, y) \Lambda_i^m\left(\varsigma_{\max} - \left(1 - \frac{\upsilon_j^n \Delta\varsigma_n + \varsigma_n}{\varsigma_{\max}}\right)\upsilon_k^m\right) f_i^m(\xi)\right]\end{aligned}$$
$$j = 2, \ldots, I_n; \quad n = 1, \ldots, N-1 \tag{A25}$$

where $\boldsymbol{f}^n = (f_1^n, f_2^n, \ldots, f_{I_n}^n)^T$ and the elements of vector $\boldsymbol{a}_j^n = (a_{j,1}^n, a_{j,2}^n, \ldots, a_{j,I_n}^n)$ are defined by Eq. A20.

Manuscript received Apr. 17, 2007, and revision received July 14, 2007.